



OPEN ACCESS

EDITED BY

Magda Pál,
HUN-REN Centre for Agricultural Research
(HUN-REN CAR), Hungary

REVIEWED BY

Selma Mlinaric,
Josip Juraj Strossmayer University of Osijek,
Croatia
Islam Frahat Hassan,
National Research Centre, Egypt

*CORRESPONDENCE

Vineet Soni
✉ vineetpbb154@gmail.com

RECEIVED 18 March 2025

ACCEPTED 16 June 2025

PUBLISHED 22 July 2025

CITATION

Shah G, Bhatt U, Singh H, Chaudhary HD and
Soni V (2025) Phytotoxic effects of cigarette
smoke on indoor plant *Epipremnum aureum*:
in vivo analysis using chlorophyll *a*
fluorescence transients.
Front. Plant Sci. 16:1595713.
doi: 10.3389/fpls.2025.1595713

COPYRIGHT

© 2025 Shah, Bhatt, Singh, Chaudhary and
Soni. This is an open-access article distributed
under the terms of the [Creative Commons
Attribution License \(CC BY\)](#). The use,
distribution or reproduction in other forums
is permitted, provided the original author(s)
and the copyright owner(s) are credited and
that the original publication in this journal is
cited, in accordance with accepted academic
practice. No use, distribution or reproduction
is permitted which does not comply with
these terms.

Phytotoxic effects of cigarette smoke on indoor plant *Epipremnum aureum*: *in vivo* analysis using chlorophyll *a* fluorescence transients

Garishma Shah, Upma Bhatt, Hanwant Singh,
Hari Dev Chaudhary and Vineet Soni*

Plant Bioenergetics and Biotechnology Lab, Mohanlal Sukhadia University, Udaipur, Rajasthan, India

Indoor air pollution from cigarette smoke, poses significant threats to plant growth and development. This study investigates the impact of cigarette smoke on the indoor plant species *Epipremnum aureum* (money plant), focusing on morphological, biochemical, and physiological aspects, with an emphasis on photosynthetic efficiency. Plants were exposed to varying concentrations of cigarette smoke (0, 2, 4, 6, 8, 10 cigarettes/day) for 15 days in controlled conditions. Key findings include a significant reduction in the mean surface area (MSA) of leaves. Chlorophyll *a* fluorescence (ChlF) analysis revealed impaired PSII photochemistry, as evidenced by reduced fluorescence yields and a significant decrease in fluorescence intensity at higher smoke exposures. Specific energy fluxes, including absorption energy (ABS/RC), trapped energy (TR₀/RC), and electron transport (ET₀/RC), showed notable reductions, while dissipated energy (DI₀/RC) increased significantly. The performance indices PI_{ABS} and PI_{CS} decreased with increasing smoke concentration and exposure duration, indicating a decline in overall photosynthetic efficiency. Principal component analysis demonstrated a distinct separation in the physiological response of plants based on exposure levels, with the highest cigarette smoke concentrations causing the most significant disruptions. The lethal dose calculations (LD₅₀ = 6.4 cigarettes/day; LD₉₀ = 9.9 cigarettes/day) highlight the severity of cigarette smoke's impact on *E. aureum*. These results underscore the detrimental effects of cigarette smoke on indoor plants, suggesting that such pollutants can significantly impair plant health and stress the importance of managing indoor air quality.

KEYWORDS

cigarette smoke, chlorophyll fluorescence, pollution, particulate matter, photosynthesis, abbreviation cigarette smoke (CS), cigarette smoke concentration (CSC), particulate matter (PM)

1 Introduction

Air pollution stands out as a paramount environmental challenge, posing significant threats to global well-being. An alarming 90% of the global population is exposed to contaminated air, resulting in approximately seven million deaths annually (Dávila-Román et al., 2021; Organization, W. H., 2018; Tarín-Carrasco et al., 2021; Zacarias and Grubert, 2021). This menace extends beyond human health, adversely impacting ecosystems and the ozone layer (de Vries, 2021; Liao et al., 2021; Rupakheti et al., 2021). The origins of air pollutants are diverse, stemming from unregulated urbanization, industrial emissions, fossil fuel consumption, and tobacco smoke (Aksoy et al., 2021). Indoor air pollution, an overlooked yet critical facet, proves to be even more hazardous, with data indicating pollution levels up to 100 times higher than outdoor air (Caselli et al., 2010; Mason et al., 2000; Wood et al., 2006). Elevated concentrations of indoor air pollutants pose severe risks to human and plant health (Brilli et al., 2018; Cetin et al., 2019). Notably, cigarette smoke in indoor environments emerges as a significant contributor, introducing a plethora of toxic compounds (Zai et al., 2012). The toll on human life is staggering, with over eight million global deaths attributed to smoke exposure, encompassing both active smoking and passive exposure (non-smokers) (Organization, W. H and others, 2015). Understanding the nature and cause of indoor pollutants, as well as distinguish them from outdoor pollutants, is essential for health risk assessment (Obore et al., 2020). It is also vital for setting regulatory strategy for indoor air quality (IAQ) and developing effective mitigation strategies to reduce human contact to air pollution, irrespective of its origin (Blount et al., 2021; Isinkaralar et al., 2024; Rajagopalan and Goodman, 2021).

Tobacco products, including cigarettes and water pipes, are major contributors to indoor air pollution. Cigarette smoke comprises two types: mainstream smoke (inhaled by the smoker) and side-stream smoke (emitted from the burning end). Environmental tobacco smoke is composed of approximately 85% side-stream smoke, which contains higher levels of toxic gases. Likewise, mainstream smoke consists of 92% gaseous elements and 8% tar. Side-stream smoke contains higher levels of toxic gases compared to mainstream smoke. Cigarette smoke consists of two phases: a tar (particulate) phase and a gas phase, which together deliver an estimated load of over 10^{17} and 10^{15} free radicals per puff, respectively, as determined through electron spin resonance (ESR) spectroscopy (Pryor and Stone, 1993). The gas phase includes carcinogens such as acrolein, acrylonitrile, hydrocyanic acid, acetaldehyde, nitrogen oxides, and carbon monoxide, and remains active for a shorter duration than the tar phase. Cigarette smoke is highly damaging to human health, causing antigenic, cytotoxic, mutagenic, and carcinogenic effects. Given that individuals spend more than 80% of their time indoors, vulnerable populations—such

as children, the elderly, and plants used for air purification—are at heightened risk from indoor air pollutant (Berglund et al., 1992).

Indoor plants are negatively affected by cigarette smoke, absorbing various toxic elements and contaminants from the air (Forster et al., 2018; Rumchev et al., 2017). Despite prohibitions on cigarette use in many countries, smoking still occurs in enclosed spaces (Fix, 2019). Indoor plants serve as effective biomonitors, absorbing pollutants and helping to assess IAQ. Several biomonitoring studies have highlighted the capacity of different plant species to capture and reflect air quality indices, including those impacted by cigarette smoke (Kumakli et al., 2017; Vimercati et al., 2016). However, prolonged exposure to smoke can result in morphological and physiological damage, such as chlorosis, necrosis, leaf curling, and reduced growth in ornamental species (Benson et al., 2019; Gushit et al., 2022; Viana, 2011). The presence of toxic metals from tobacco smoke necessitates monitoring IAQ at its source. Indoor plants face stresses from IAQ, water availability and concentration of smoke, impacting their ability to absorb toxic metals. Research indicates that ornamental species growing in smoky areas may experience leaf degradation due to this absorption. PM also attaches to various organs of plants such as hairy leaves or bark (Hatami-Manesh et al., 2021) which produce ill effect in plant development. Because leaves are the organs with air entry and exit through their stomata, and they interact with air the most. Leaves, being the primary interface for gas exchange, play a critical role in pollutant uptake. The extent of toxic metal absorption is influenced by the physical and chemical properties of the metals, plant species, organ morphology, surface area, surface texture, environmental conditions, and exposure duration (Shahid et al., 2019). PM also accumulates on rough surfaces such as hairy leaves or bark, further contributing to physiological stress (Hatami-Manesh et al., 2021). However, the accumulation of toxins may vary on the basis of plant organ and species of plants (Gorena et al., 2020). The differences among tobacco products and plant species can provide insights into air pollution effects and help identify potential bio-monitor species. Their exposure to smoke can lead to leaf degradation and stress. Numerous plant studies have also been conducted on bio-monitoring of toxins from cigarette smoke (Kumakli et al., 2017; Vimercati et al., 2016), but the direct physiological effects of cigarette smoke exposure on indoor plants remain underexplored.

The present investigation aims to assess the effects of cigarette smoke on plants physiology and morphology of the indoor plant species *Epipremnum aureum* (money plant). This species is chosen for its widespread presence and heightened sensitivity, making it a frequent subject in experimental studies. The central hypothesis is that continuous and prolonged exposure to cigarette smoke leads to measurable and dose-dependent physiological and morphological stress in *E. aureum*. These stress responses introduce adverse effects like reduced photosynthetic efficiency, loss of chlorophyll content, leaf deformation, and signs of oxidative damage.

Chlorophyll *a* fluorescence (ChlF) is employed as a widely accepted and non-invasive technique to detect plant stress conditions, often integrated with other physiological and chemical variables (Miranda et al., 2020; Percival et al., 2006). This provides a

Abbreviations: CS, Cigarette Smoke; CSC, Cigarette Smoke Concentration; PM, Particulate Matter; CS, Reaction Centre; PSI, Photosystem I; PSII, Photosystem II; LHClI, Light-Harvesting Complex II.

quantitative measure of oxygenic photosynthesis (Ashraf et al., 2019). Exposure to CS disrupts photosynthesis through chemical interactions with proteins, leading to an escalation in reactive oxygen species generation (Dobaradaran et al., 2021; Yadav, 2010). These findings will provide a more precise understanding of how smoke pollutants affect plants growth and development.

2 Materials and methods

2.1 Plant material

Epipremnum aureum plants were purchased from a local nursery in Udaipur, India. The plant specimens were identified by Dr. Vineet Soni using morphological characteristics such as climbing habit, presence of aerial roots that adhere to surfaces, and leaf morphology, heart-shaped and irregularly pinnatifid in mature plants, entire in juvenile plants, and trailing stems. The identification was further confirmed using the taxonomic key described in Basu et al. (2014) and cross-referenced with regional floras such as Bennet et al. (1987) for Araceae species. After purchasing plant age was around five weeks old, plants were kept in growth chamber at $28 \pm 3^\circ\text{C}$ and 70% relative humidity under a 16:8 h photoperiod (day/night) for 24 h at Plant Bioenergetics and Biotechnology Laboratory, MLS University, Udaipur, India. Following acclimation, the plants were cultivated for an additional two weeks in an open greenhouse under natural light conditions with supplemental growth materials. The soil used had a composition of 40–50% clay, 25–30% silt, and 25–30% sand, with a pH level of 7.10 and an organic matter content of 0.64% (w/w). During this cultivation period, the average temperature ranged from $30\text{--}32^\circ\text{C}$ with a 12 h light/12 h dark photoperiod. At the time of experimentation, plants were approximately 7 weeks old and had reached a height of about 15 cm, indicating juvenile developmental stage. During the experimental phase, plants were kept under controlled laboratory conditions at $28 \pm 3^\circ\text{C}$ temperature, 75% relative humidity, and a 16:8 h photoperiod (day/night). A fluorescent lamp emitting photosynthetically active radiation (400–700 nm) at an intensity of approximately $50 \mu\text{mol m}^{-2} \text{s}^{-1}$ was used as the light source. Five morphologically similar individuals were selected and used as biological replicates for each treatment.

2.2 Experiment setup

Six experimental wooden chambers were designed, each with a floor area of approximately 0.46 m^2 (5 square feet) and a height of 2 meters, resulting in an internal volume of approximately 0.92 m^3 per chamber. Each chamber was maintained under standard temperature and pressure (STP) conditions with a controlled photoperiod of 16:8 h light/dark. Six different treatments were established based on daily cigarette smoke concentration (CSC/Day): 0 (control), 2, 4, 6, 8, and 10 cigarettes per day, respectively. Each treatment had five biological replicates.

The average distance between each plant and the cigarette smoke source (artificial pump) was consistently maintained at 0.91 meters (3 feet). A standardized cigarette brand (Gold Flake Kings, ~70 mm length) was used. Cigarette smoke was generated using a custom-made artificial smoking device (flow rate ~17.5 mL/min) that mimicked human puffing intervals, burning each cigarette over ~5–7 minutes, according to the assigned treatment concentration. Each cigarette was puffed once every 30 seconds for 6–7 minutes. Smoke was released into the chamber via a small vent to ensure uniform dispersion. The experiment lasted 15 days, and measurements were recorded every third day.

2.3 Measurement of morphological parameters

To assess specific morphological variability in *E. aureum* exposed to CSC, the mean surface area (MSA) and mean damage area (MDA) were determined using Fiji-Image J software, an open-source tool for advanced image processing and scientific analysis (<https://imagej.net/Fiji>). Seven images were captured for each plant at three-day intervals over a 15-day period using a Nikon D7500 DSLR camera (20.9 MP resolution) from a distance of 70 cm under diffused light conditions.

2.4 Measurement of chlorophyll *a* fluorescence

Chlorophyll *a* fluorescence (ChlF) was measured using the Handy PEA fluorimeter from Hansatech Instruments Ltd., England. Prior to measurement, plants were dark-adapted for 50–60 minutes at 26°C . The ChlF signals were analyzed with BioLyzer v.3.0.6 software, developed by the Laboratory of Bioenergetics at the University of Geneva, Switzerland. The experiments were conducted in five replicates and repeated three times to ensure accuracy. The JIP-test method was employed to calculate various phenomenological and biophysical parameters, quantifying the behaviors of photosystem I (PSI) and photosystem II (PSII). The polyphasic ChlF rise, known as the OJIP curve, provided valuable insights into photosynthetic fluxes, with numerous parameters derived from it (Strasser, 1992; Strasser et al., 2000). Table 1 presents the definitions, formulas, and abbreviations for the JIP-test parameters used in this study.

2.5 Measurement of chlorophyll content

The Arnon, (1949) method was applied to ascertain the total chlorophyll content in *E. aureum* plants under CS. Fresh leaves were crushed in 80% acetone, and the resulting extract was collected in a 3 mL vial. The extract was then subjected to cold centrifugation at 4°C and 5000 rpm for five minutes. For the quantification of chlorophyll *a* (chl *a*) and chlorophyll *b* (chl *b*), the supernatant obtained after centrifugation was analyzed using a spectrophotometer at

TABLE 1 The JIP-test parameters, along with their respective abbreviations, formulas, and definitions, are presented.

BASIC PARAMETERS CALCULATED FROM THE EXTRACTED DATA	
$F_0 \cong F_{50\mu s} \text{ or } F_{20\mu s}$	Fluorescence when all PSII RCs are open (Tsimilli-Michael, 2020)
$T_{FM} = t_{F_{MAX}}$, t for F_M	Time (in ms) to reach maximal fluorescence F_M (Stirbet et al., 2018; Tsimilli-Michael, 2020)
F_M	Maximal fluorescence, when all PSII RCs are closed (Stirbet et al., 2018; Tsimilli-Michael, 2020)
BIOPHYSICAL PARAMETERS DERIVED FROM THE BASIC PARAMETERS	
<i>Specific energy fluxes (per RC : QA-reducing PSII RC), in ms^{-1}</i>	
$ABS/RC = M_O \times (1/V_j) \times (1/\phi_{p_0})$	Absorption flux (exciting PSII antenna Chl a molecules) per RC (also used as a unit-less measure of PSII apparent antenna size) (Strasserf and Srivastava, 1995; Stirbet et al., 2018; Tsimilli-Michael, 2020)
$TR_O/RC = M_O \times (1/V_j)$	Trapped energy flux (leading to Q_A reduction), per RC (Tsimilli-Michael, 2020)
$ET_O/RC = M_O \times (1/V_j) \times (1 - V_j)$	Electron transport flux (further than Q_A^-), per RC (Tsimilli-Michael, 2020)
$DI_O/RC = ABS/RC - TR_O/RC$	Dissipated energy flux per RC (at $t = 0$) (Tsimilli-Michael, 2020)
<i>Phenomenological energy fluxes (per CS: QA-reducing PSII cross section), in ms^{-1}</i>	
$TR_O/CS_M = (F_v/F_M) (ABS/CS_M)$	Trapped energy flux (leading to Q_A reduction) per RC (Tsimilli-Michael, 2020)
$ET_O/CS_M = (F_v/F_M) (1 - V_j) (ABS/CS_M)$	Electron transport flux (further than Q_A^-) per RC (Tsimilli-Michael, 2020)
$DI_O/CS_M = (ABS/CS_O) - (TR_O/CS_M)$	Total energy dissipated per reaction center (RC) (Tsimilli-Michael, 2020)
$ABS/CS_M \cong F_0$	Absorbed photon flux per excited PSII cross section at time zero (Tsimilli-Michael, 2020)
<i>Quantum yields and efficiencies</i>	
$\phi_{p_0} \cong TR_O/ABS = [1 - (F_0/F_M)]$	Maximum quantum yield for primary photochemistry (Tsimilli-Michael, 2020)
$\phi_{E_0} \cong ET_O/ABS = [1 - (F_0/F_M)] \times (1 - V_j)$	Quantum yield for electron transport (ET) (Strasserf and Srivastava, 1995)
$\psi_{E_0} \cong ET_O/TR_O = (1 - V_j)$	Efficiency/probability that an electron moves further than Q_A^- (Strasserf and Srivastava, 1995)
$\phi_{D_0} = F_0/F_M$	Quantum yield (at $t = 0$) of energy dissipation (Strasserf and Srivastava, 1995)
<i>Performance indexes</i>	
$PI_{ABS} = \frac{1 - (F_0/F_M)}{M_O/V_j} \times \frac{F_M/F_0}{F_0} \times \frac{1 - V_j}{V_j}$	Performance index for energy conservation from photons absorbed by PSII until the reduction of intersystem electron acceptors (Strasserf and Srivastava, 1995; Stirbet et al., 2018; Tsimilli-Michael, 2020)
$PI_{CS} = \frac{ABS}{CS} \times \frac{1 - (F_0/F_M)}{M_O/V_j} \times \frac{F_M/F_0}{F_0} \times \frac{1 - V_j}{V_j}$	Performance index on cross section basis (Strasserf and Srivastava, 1995; Stirbet et al., 2018; Tsimilli-Michael, 2020)

wavelengths of 663 nm and 645 nm, respectively. The absorbance values obtained were then used in the following formula to estimate the total chlorophyll content:

$$\begin{aligned}
 & \text{Total chl. content} \left(\frac{mg}{g} \right) \\
 & = (20.2 \times A_{663} + 8.02 \times A_{645}) \times \frac{V}{1000 \times W}
 \end{aligned}$$

Where A_{663} and A_{645} are the absorbance values at their respective wavelengths, V is the volume of the extract (in mL), and W is the weight of the plant material used for extraction (in g).

2.6 Statistical analysis

Statistical analyses were conducted using ANOVA with Tukey’s HSD test ($p = 0.05$) compare the effects of different cigarette smoke concentrations on plant physiological and morphological parameters. A significance level of $p \leq 0.05$ was used to determine

statistically meaningful differences among treatments. Before conducting ANOVA, assumptions of normality (Shapiro–Wilk test) and homogeneity of variance (Levene’s test) were confirmed. Each treatment consisted of five biological replicates (i.e., five individual plants per treatment), and measurements were taken from each replicate. The analysis was conducted using SPSS software (version 22.0). Only statistically significant differences ($p \leq 0.05$) were represented in the figures. For the heat map, values were normalized and scaled from 1 to 100, with high values (100%) represented in brown, medium values (50%) in orange, and low values (1%) in yellow. Principal Component Analysis (PCA) was carried out using Origin Pro 2018 to uncover patterns and variations in the data, based on eigenvalue decomposition of the data correlation matrix. Correlations between parameters were assessed using a grid correlation matrix, with results visualized using a color scale from +1 to -1, facilitated by Python software (Gomez-Flores et al., 2023; Sangani et al., 2019). Probit analysis was performed with SPSS (version 22.0) to estimate the lethal doses (LD_{50} and LD_{90}). In this study, mortality was defined as complete

leaf necrosis ($\geq 90\%$ of leaf area affected), which was standardized across treatments. A Chi-square test was employed to compare mortality ratios between experimental and control groups at different concentrations, ensuring the coefficient of variance was less than 7%.

3 Results

The growth of *E. aureum* was significantly affected by the CS, which caused modulation of the plant's photosynthetic process. To investigate this phenomenon, the current study explored the impact of CSC on various parameters on *E. aureum* including morphological parameters, chlorophyll fluorescence, specific energy fluxes, phenomenological energy fluxes, and performance indexes.

3.1 Morphological parameters

The mean surface area (MSA) of *E. aureum* showed a progressive and significant decrease with increasing concentrations of CS, as presented in Table 2. The MSA was measured at regular intervals over 15 days and expressed in cm^2 . On day 0, the initial MSA for all treatments was approximately similar ($\sim 10.4\text{--}10.7\text{ cm}^2$). However, by the 9th day, plants treated with 10 CSC exhibited a drastic reduction in MSA to $1.56 \pm 0.187\text{ cm}^2$, representing a nearly 85% decline compared to the control ($10.656 \pm 0.011\text{ cm}^2$). By the 15th day, the MSA further decreased to $0.452 \pm 0.168\text{ cm}^2$ under 10 CSC exposures.

In contrast, the mean damage area (MDA) was calculated using mean surface area value as the difference between the initial surface area (day 0) and the final surface area (day 15). The MDA increased proportionally with CS concentration, indicating progressive leaf damage. The most extensive damage was observed in the 8 CSC and 10 CSC treatments, where the MDA reached 8.462 cm^2 and 10.312 cm^2 , respectively. These results are visually represented in Figure 1, where leaves under 8 CSC (E) and 10 CSC (F) treatments show complete necrosis and collapse, correlating with the near-total

reduction in leaf surface area. This confirms the severe phytotoxic effects of CSC at higher concentrations.

3.2 Total chlorophyll content

The total chlorophyll content in plants over different exposure days under various CS treatments showed in Figure 2B. The control group consistently showed the highest chlorophyll levels across all days. As the duration increased, a gradual decline in chlorophyll content was observed in all treatment groups (3 to 15). This reduction was more pronounced in higher concentrations, particularly in 12th and 15th. By the final day, 15th showed the lowest chlorophyll levels, indicating severe degradation. The consistent downward trend highlights the negative impact of CS on chlorophyll synthesis. The data also reflect a time- and dose-dependent phytotoxic effect. Minimal error bars suggest reliable and reproducible measurements. Leaf impression showing green color variation estimate through biolyzer software present in Figure 2A. The green intensity of each leaf impression correlates with the estimated total chlorophyll level based on image fluorescence data.

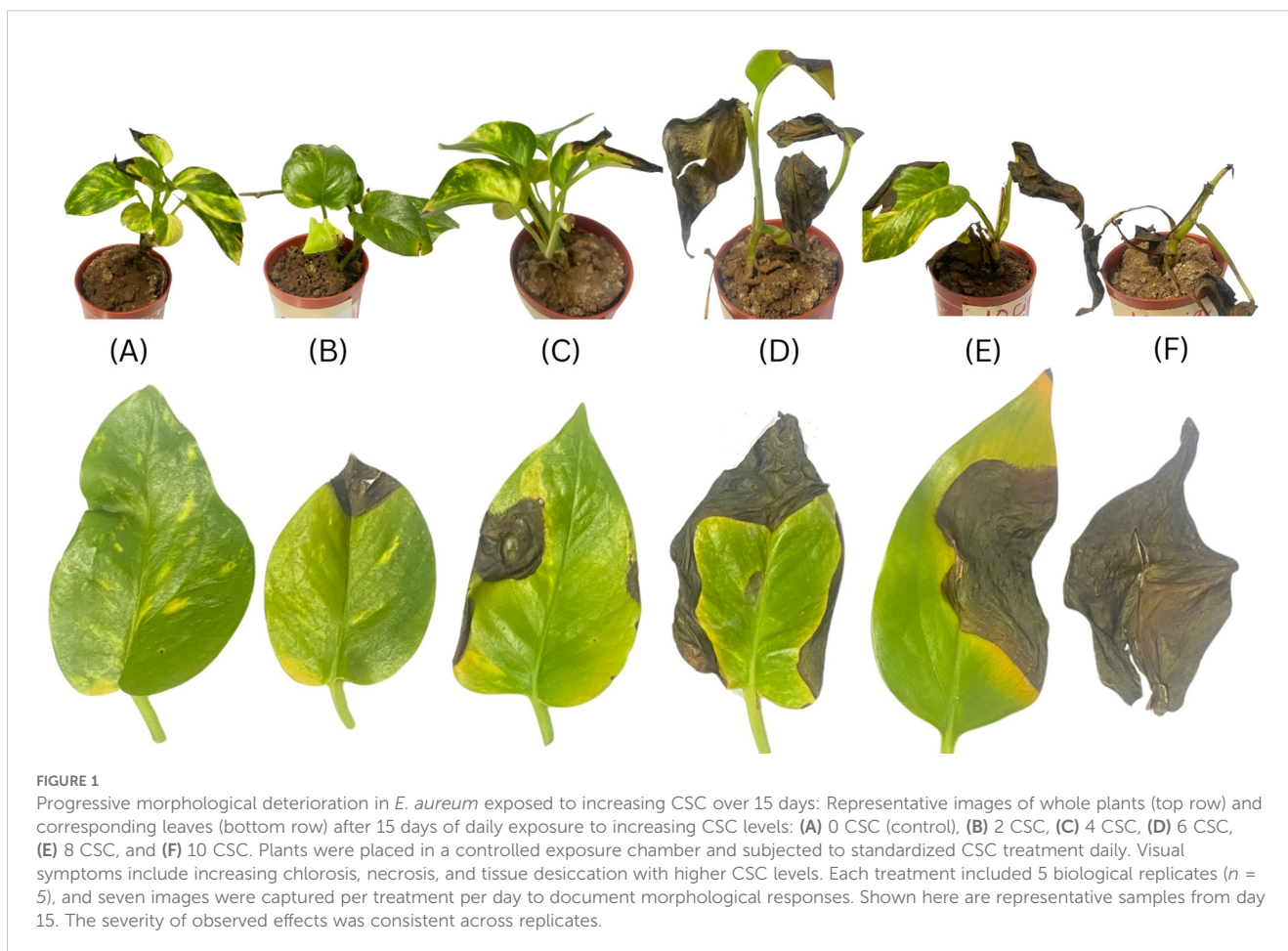
3.3 Chlorophyll a fluorescence kinetics

The chlorophyll fluorescence (ChlF) of *E. aureum* was assessed 3-days after exposure to CSC, revealing a typical OJIP induction curve when plotted on a logarithmic time scale. As the CSC increased, the fluorescence yield at J, I, and P steps were decreased. In control plants, two intermediate peaks, F_j (fluorescence intensity at 2 ms) and F_I (fluorescence intensity at 300 ms), were observed between F_0 and F_M . CSC exposure led to a reduction in PSII photochemistry and electron transport activity, especially at the highest CSC concentrations. Notably, on the 3rd and 6th days, the fluorescence intensity at 4 CSC and 6 CSC was higher than in the control conditions, but by the 9th, 12th, and 15th days, the intensity had decreased to 25% of the control levels. Furthermore, after the 12th day, the fluorescence intensity in plants exposed to 8 CSC and 10 CSC conditions had nearly diminished to zero. This fluorescent intensity is representing in Figure 3 and Supplementary Table 1.

TABLE 2 Change in leaf area define as a mean surface area with the increasing CSC with days with $X \pm S$ for five replicate measurements at a 95% level of confidence.

Mean Surface Area (cm^2)						
CSC	Day 0	Day 3	Day 6	Day 9	Day 12	Day 15
0	10.556 ± 0.011^a	10.55 ± 0.097^{ab}	10.596 ± 0.095^b	10.656 ± 0.011^c	10.696 ± 0.184^a	10.636 ± 0.128^c
2	10.674 ± 0.137^a	10.2 ± 0.137^{abc}	10.2 ± 0.137^b	10.2 ± 0.185^{cd}	8.418 ± 0.307^a	8.2 ± 0.137^c
4	10.718 ± 0.378^a	9.26 ± 0.470^b	8.51 ± 0.503^{ab}	7.9 ± 0.248^d	6.946 ± 0.714^{ab}	6.66 ± 0.750^c
6	10.434 ± 0.470^a	8.51 ± 0.750^b	6.66 ± 0.776^{ab}	5.86 ± 0.147^d	4.032 ± 0.677^{abc}	3.476 ± 0.355^{cd}
8	10.43 ± 0.231^a	6.66 ± 0.176^{bc}	5.86 ± 0.677^{ab}	4.032 ± 0.171^d	2.954 ± 0.246^{abc}	1.968 ± 0.430^{cd}
10	10.764 ± 0.150^a	6.66 ± 0.376^{bc}	5.86 ± 0.472^{ab}	1.56 ± 0.187^d	1.56 ± 0.472^c	0.452 ± 0.168^{bc}

Different letters indicate a significant difference ($P \leq 0.05$).



3.4 Biophysical parameters

CSC has been observed to reduce both the minimal fluorescence intensity (F_0) and the maximal fluorescence intensity (F_M). One-way ANOVA followed by Tukey's HSD test ($p < 0.05$) confirmed statistically significant differences between treatment groups, particularly at higher CSC concentrations, indicating dose-dependent phytotoxic effects. F_0 is the fluorescence measured at 50 μs when the primary quinone acceptor (Q_A) is in its oxidized state. The efficiency of photosynthesis in plants is closely associated with the maximum primary yield of PSII photochemistry, as indicated in Figure 4. This ratio reflects the rates at which excited chlorophyll pigments undergo photochemical and non-photochemical deactivation. At concentrations of 4 CSC and 6 CSC, F_M values initially increased on the 6th and 9th days, but subsequently decreased to about 90% of the control values. In contrast, changes in F_0 values were minimal.

3.5 Quantum yield

The introduction of CSC to plants led to a slight reduction in the quantum yield of primary photochemistry (ϕP_0) and electron transport (ϕE_0), ϕP_0 reflects the efficiency of energy conversion at

the primary photochemical step of PSII, while ϕE_0 indicates the efficiency of electron transport beyond Q_A^- both are indicators of the photosynthetic efficiency of active PSII RC. This trend is evident in Figure 5. The minimal values of ϕP_0 and ϕE_0 , approximately one fourth of the control, were recorded when *E. aureum* was exposed to 10 CSC. These values continuously decreased as the exposure duration and smoke concentration increased Figures 5A–C. In contrast, the quantum yield of dissipation (ϕD_0) exhibited a continuous increase with rising CSC levels, showing an approximately two-fold increase compared to the control under the 10 CSC condition on the 4th day. Furthermore, the ϕD_0 value increased up to four times by the last day of the experiment under the 10 CSC condition. “These dynamics in energy fluxes are visually summarized in a ‘raindrop regression model’ diagram (Figure 5), where individual photochemical parameters (ϕP_0 , ϕE_0 , and ϕD_0) are plotted over time and across CSC treatments, allowing for comparative visualization of their temporal and dose-dependent behavior. To support these visual interpretations, statistical analyses were performed using one-way ANOVA followed by Tukey's *post hoc* test. The differences observed in ϕP_0 , ϕE_0 , and ϕD_0 across treatment groups were found to be statistically significant ($p < 0.05$), confirming that the variations in quantum yields are not due to random chance but are a result of CSC exposure.

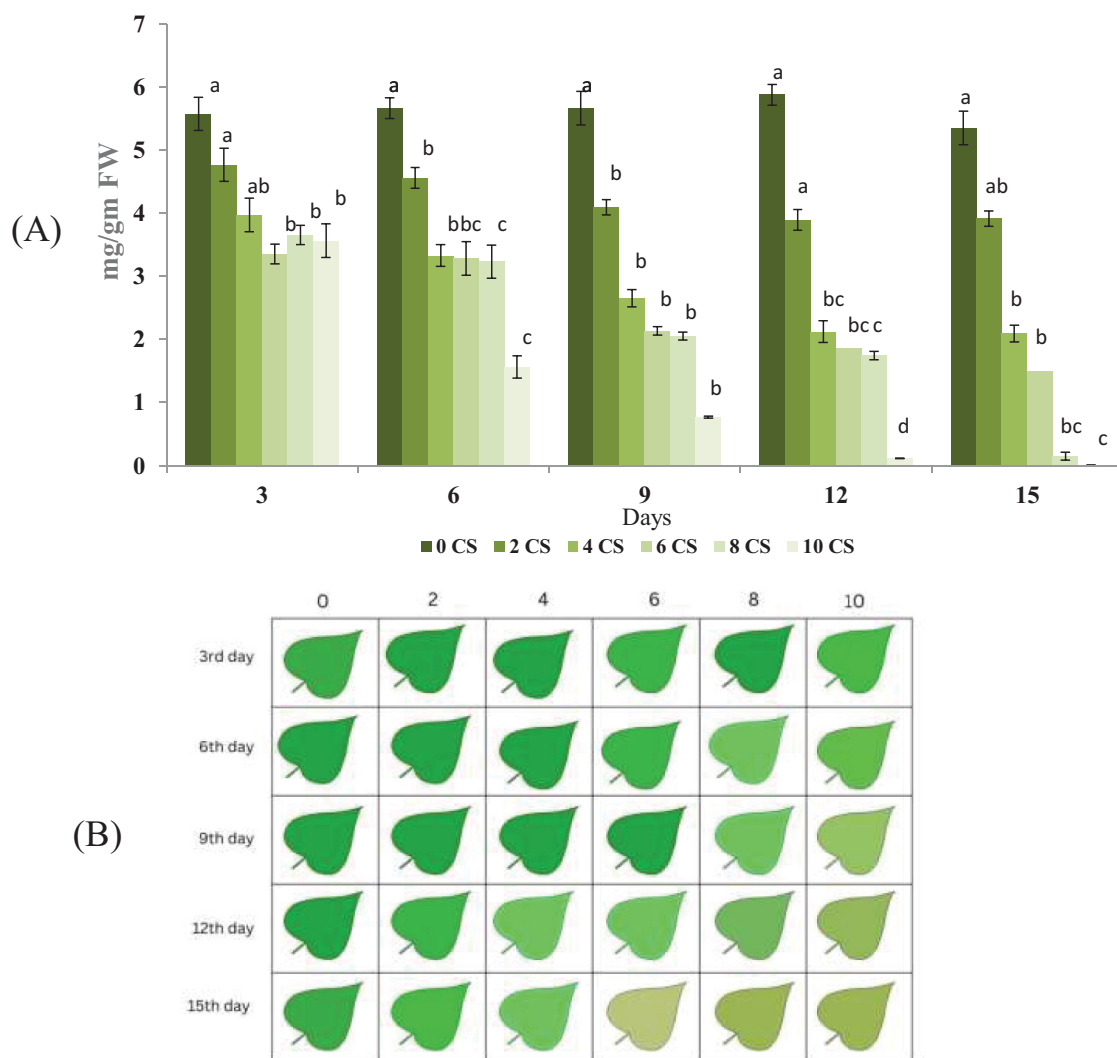


FIGURE 2 Chlorophyll content decline and visual color transition in *E. aureum* under increasing CSC over 15 days: **(A)** Total chlorophyll content (mg/g FW) measured in leaves of *E. aureum* exposed to 0, 2, 4, 6, 8, and 10 CSC for 15 days, recorded at 3-day intervals (Day 3, 6, 9, 12, 15). Chlorophyll estimation was performed using standard Arnon (1949) methods. Data represent mean \pm SE of $n = 5$. Different lowercase letters above bars indicate statistically significant differences among treatments at each time point (ANOVA, $p < 0.05$, Tukey's HSD). **(B)** Representative color-coded chlorophyll index of a single leaf under different CSC treatments (0–10) over five time points. A clear reduction in chlorophyll intensity and uniformity is visible with increasing CSC and duration of exposure.

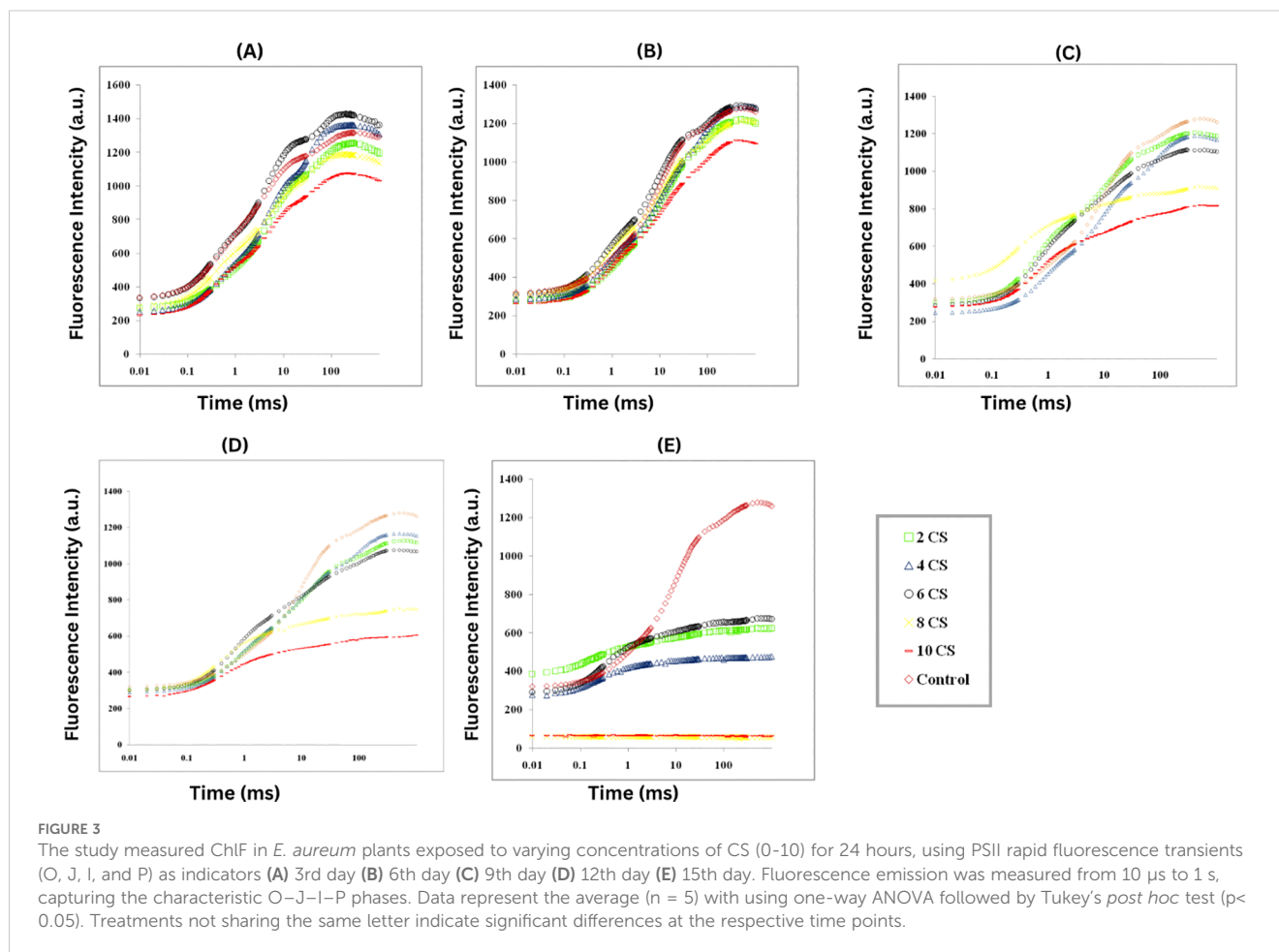
3.6 Specific energy fluxes

The study analyzed the photosynthetic performance of active PSII RC in *E. aureum* under varying CSC by examining specific energy fluxes, including absorption energy (ABS/RC), trapped energy (TR₀/RC), electron transport (ET₀/RC), and dissipated energy (DI₀/RC) flux per reaction center, as shown in area plot in Figure 6. The results indicated significant increase in ABS/RC at 4 and 6 CSC conditions up to the 9th day, followed by a declining trend with increasing concentration and exposure duration. Minimal changes were observed in the values of TR₀/RC and ET₀/RC till the 9th day, after which a gradual reduction was noted with increasing days and CSC. By the last day, TR₀/RC and ET₀/RC values had decreased by approximately 49.89% and 76.78% from

the control, respectively, indicating a huge loss in energy trapping and electron transport efficiency. Conversely, DI₀/RC displayed a substantial sequential increase, with approximately a fivefold increment observed in plants treated with 10 CSC compared to the control (Figure 6).

3.7 Phenomenological energy fluxes

The impact of CSC-induced stress on *E. aureum* was assessed by examining changes in phenomenological energy fluxes, including absorption (ABS/C_{Sm}), trapped energy (TR/C_{Sm}), electron transport (ET/C_{Sm}), and dissipated energy (DI/C_{Sm}) flux per cross-section. Across all time points, increasing CSC concentrations



led to a consistent and significant reduction in ABS/CSm, TRo/CSm, and ETo/CSm, with a concurrent increase in DIo/CSm. All these parameters exhibited significant reductions with increasing CSC levels in *E. aureum*. Specifically, under the 10 CSC condition on the 15th day, ABS/CSm, TR/CSm, and ET/CSm, decreased by 50.13%, 75.89%, and 49.15%, respectively. Whereas DI/CSm increased by 82.60%, in the last day of CSC exposure compared to the control represent in Figure 7. Statistical analysis (one-way ANOVA, $p < 0.05$) confirmed significant differences across CSC concentrations.

3.8 Performance index

In order to assess the effects of CSC on the overall performance of photosynthesis, PI_{ABS} (performance index on absorption basis) and PI_{CS} (performance index on cross section basis) were measured in *E. aureum* plants subjected to different intensities of CSC stress. The results showed that CSC had a significant effect on PI_{ABS} and PI_{CS} , with both parameters decreasing continuously as the CSC increased. In the box bar plot Figure 8A, PI_{ABS} and PI_{CS} were representing with the days. The toxicity of cigarette smoke increased over time, resulting in a progressive decline in photosynthetic performance, as reflected by reductions in both

parameters (PI_{ABS} and PI_{CS}) across the days. Along this the value of PI_{ABS} and PI_{CS} were 10 times lower compared to the initial day of exposure than the start day. In Figure 8B, PI_{ABS} and PI_{CS} were calculated on the axis of increasing smoke concentration, significant declining pattern were observed. Nevertheless in cluster bar graph Figures 8A, B, combine result was present with the time and CSC scale. The results of the PCA analysis showed that the first two principal components for day 3 Figure 9A, Dim 1 and Dim 2, explain 98.56% of the cumulative variation in the ChlF parameter under CSC induced stress in *E. aureum*. On day 3, the loading plot shows that several JIP-test parameters—including ET_0/RC , ET_0/CSm , PI_{CS} , ABS/RC , TR_0/RC , DI_0/RC , TR_0/CSm , ABS/CSm , DI_0/CSm , ϕD_0 , F_0 , and F_M —are grouped primarily in quadrant I. In contrast, performance indices and quantum yields such as PI_{ABS} , ϕP_0 , and ϕE_0 are located in quadrant II. Notably, the 10 CSC treatment group is distinctly separated from most JIP parameters, indicating reduced correlation under high CSC stress.

By the 15th day (Figure 9B), PC1 and PC2 explain 98.28% of the cumulative variation. The distribution of JIP parameters remains largely consistent with day 3, still concentrated in quadrants I and II. However, unlike day 3, no chlorophyll fluorescence parameters are correlated with the 8 CSC and 10 CSC treatments, which are positioned distantly from the major clusters. This separation

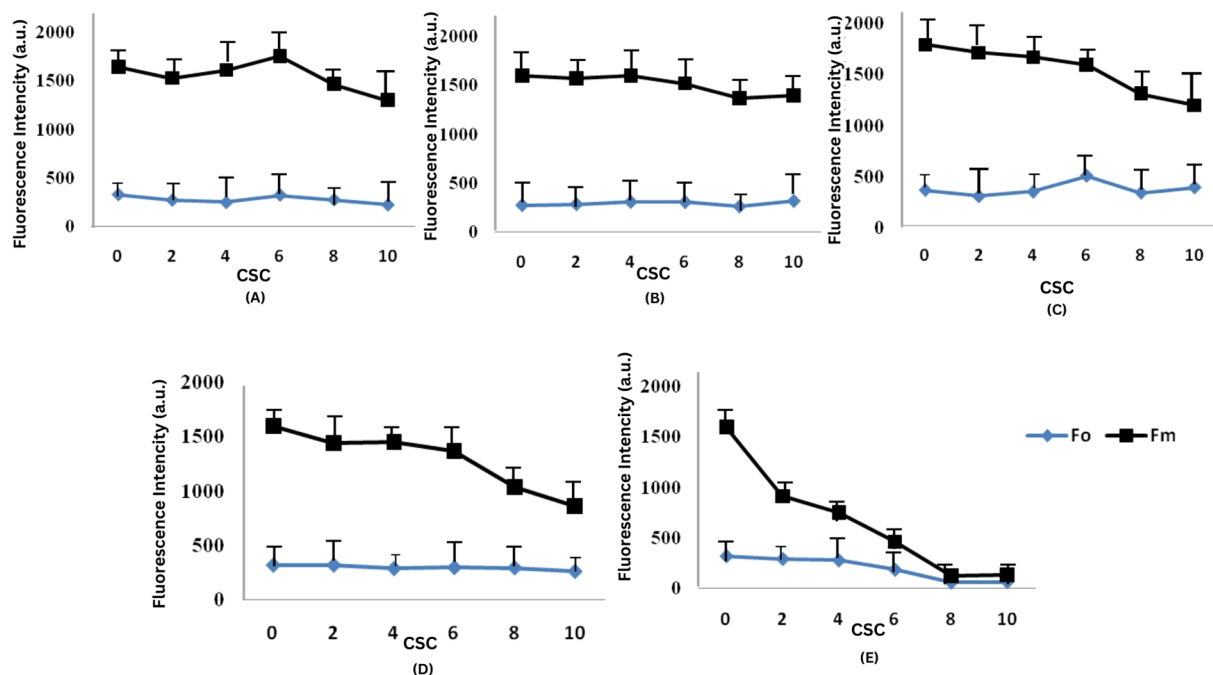


FIGURE 4
 Effect of CSC on minimal (F_0) and maximal (F_m) chlorophyll fluorescence in *E. aureum*. The figure shows the changes in initial (F_0) and maximum (F_m) chlorophyll fluorescence intensity under varying concentrations of CSC: 0, 2, 4, 6, 8, and 10 CS over a 15-days (A) Day 3, (B) Day 6, (C) Day 9, (D) Day 12, and (E) Day 15. One-way ANOVA ($n = 5$), followed by Tukey's *post hoc* test ($p < 0.05$).

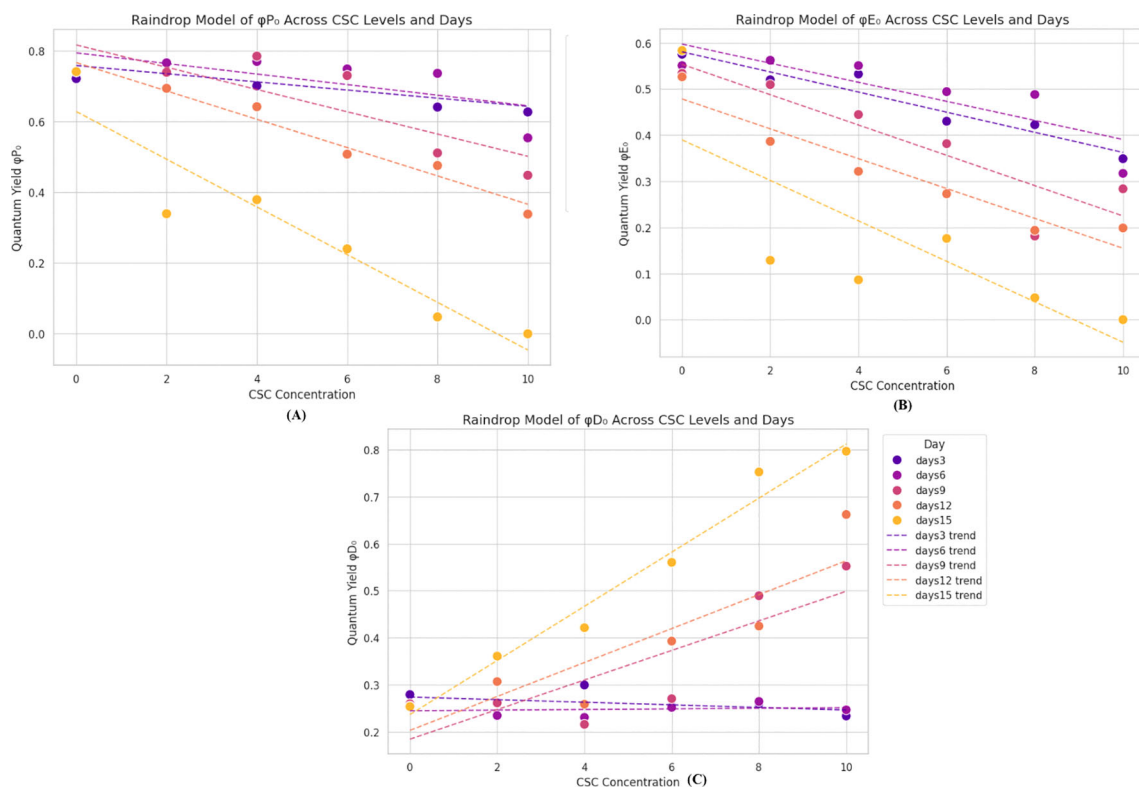


FIGURE 5
 Raindrop regression models showing changes in chlorophyll fluorescence parameters in *E. aureum* exposed to increasing CSC concentrations (0–10) over 15 days. (A) ϕP_0 (primary photochemistry) and (B) ϕE_0 (electron transport) decreased with higher CSC and time. (C) ϕD_0 (energy dissipation) increased, indicating enhanced protective response. Data represent means of five replicates ($n = 5$); trendlines show progression over time (Day 3–15). Significant differences were determined by two-way ANOVA with Tukey's test ($p < 0.05$).

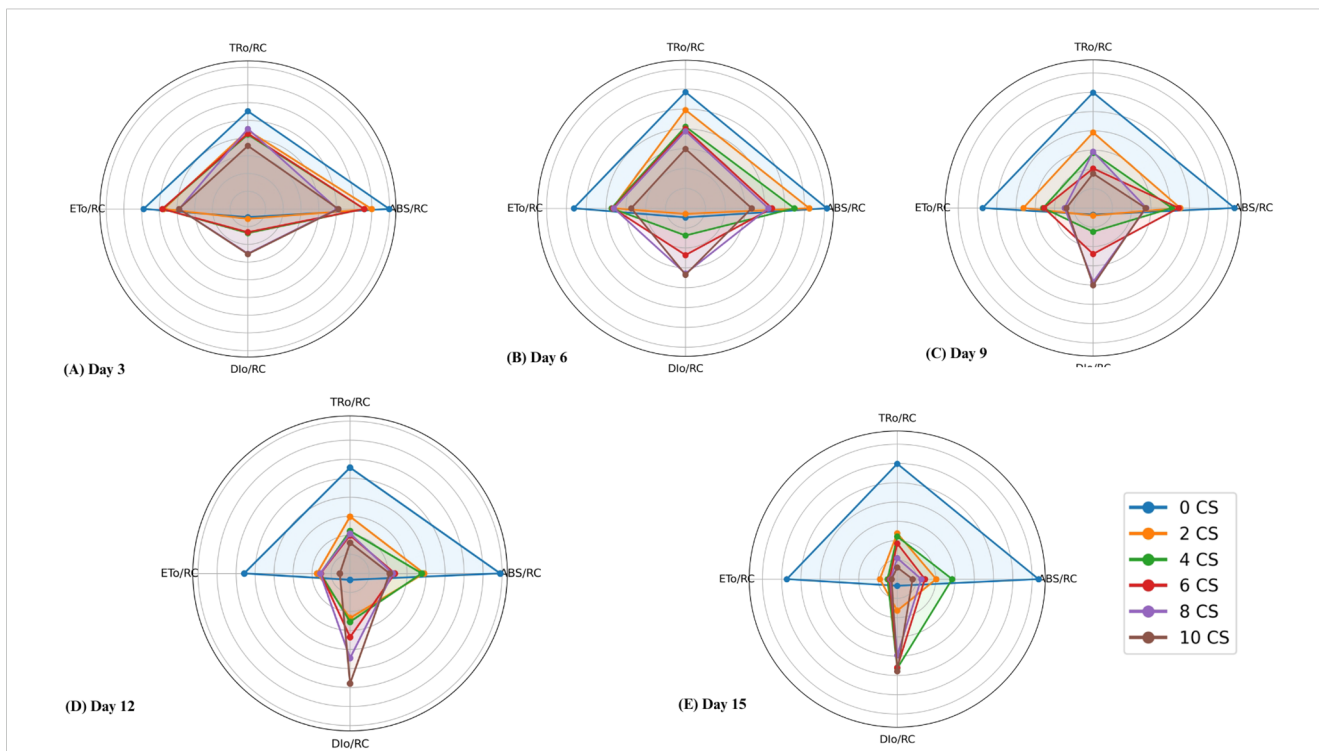


FIGURE 6 Radar plots illustrating specific energy fluxes per reaction center –ABS/RC (absorbed energy), TR_o/RC (trapped energy), ET_o/RC (electron transport), and DI_o/RC (dissipated energy) in *Epipremnum aureum* leaves across different exposure durations: **(A)** Day 3, **(B)** Day 6, **(C)** Day 9, **(D)** Day 12, and **(E)** Day 15. As the concentration of cigarette smoke (CS) and exposure time increase, energy absorption, trapping, and electron transport (ABS/RC, TR_o/RC, ET_o/RC) decrease significantly, while energy dissipation (DI_o/RC) increases sharply ($p < 0.05$).

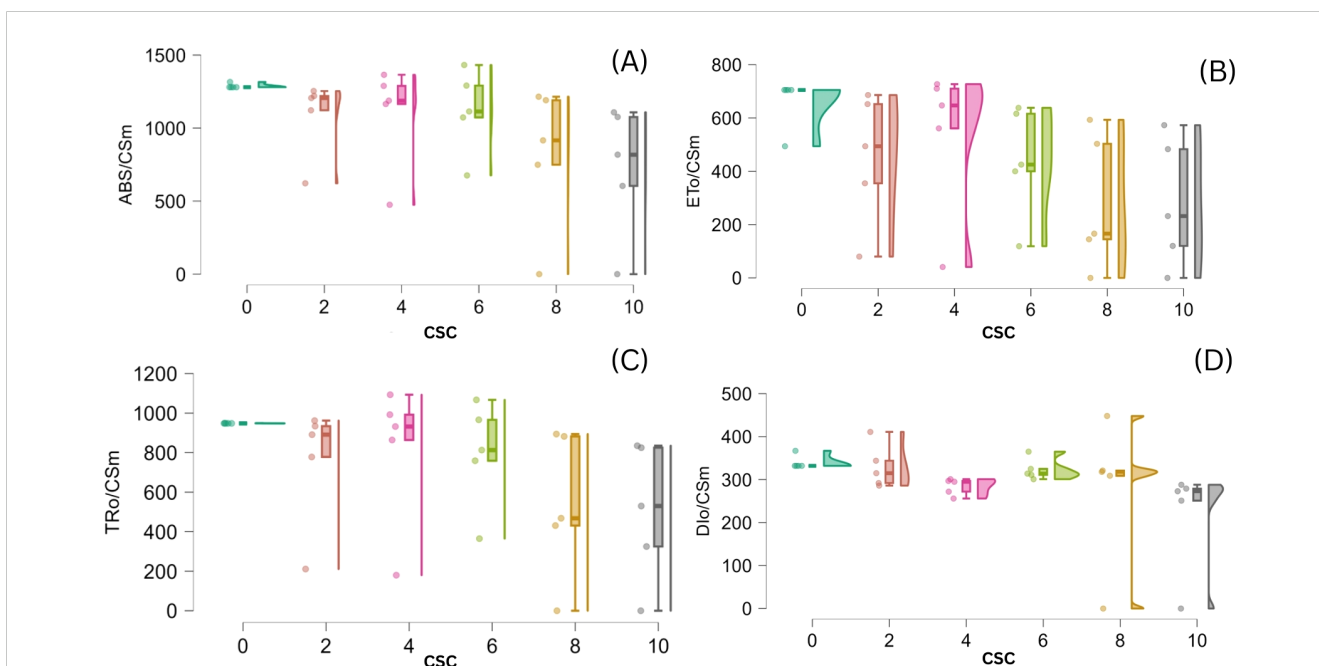
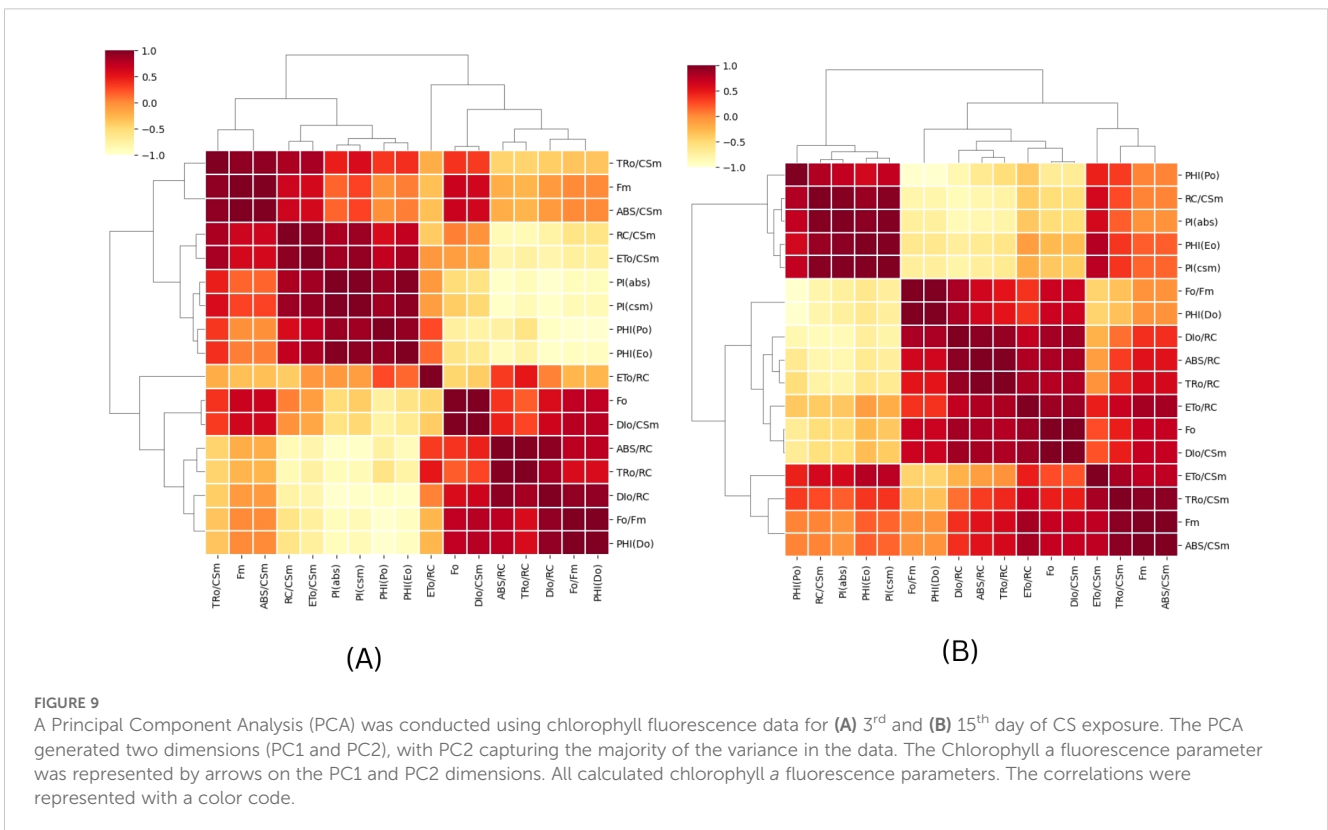
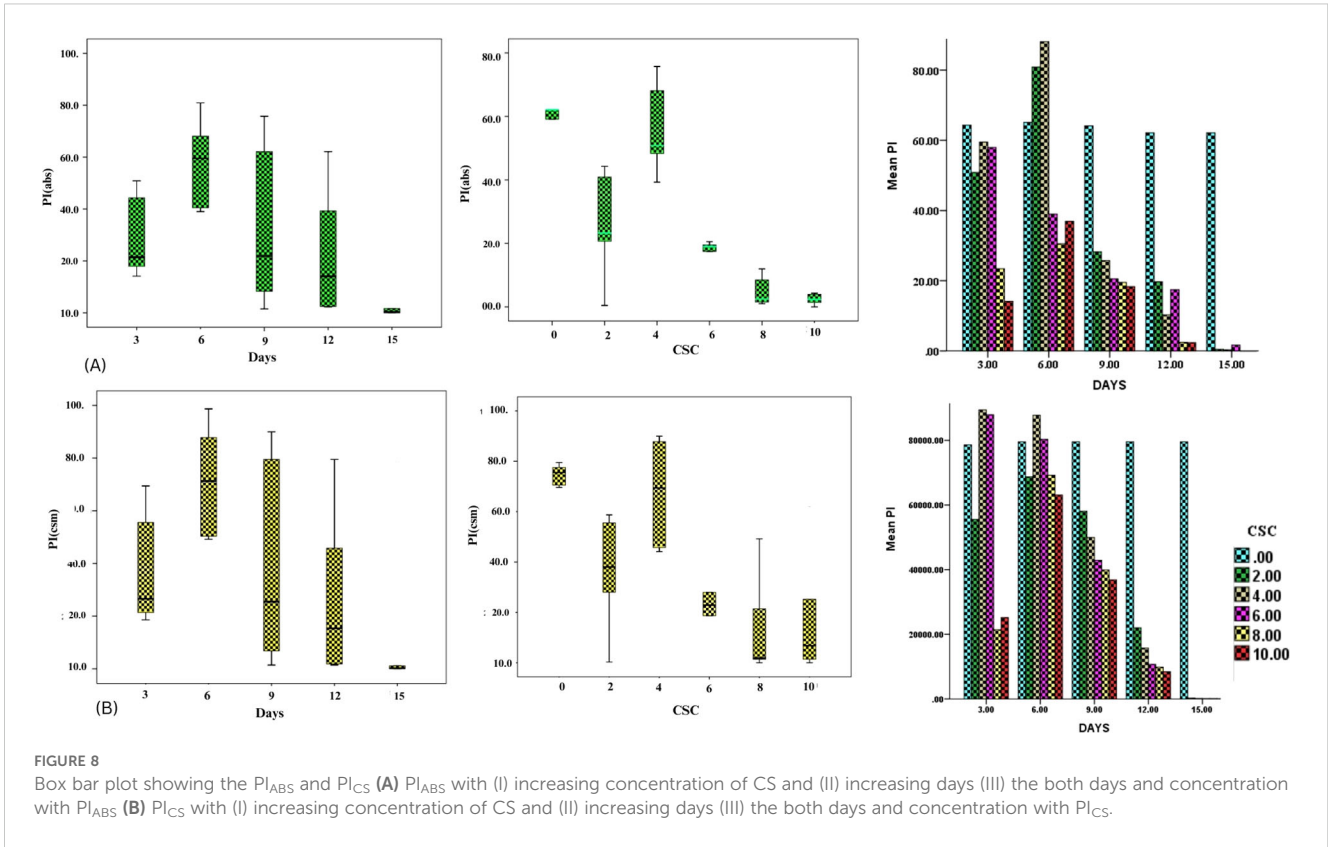


FIGURE 7 Violin (regression raindrop) plots depicting the effect of increasing cigarette smoke concentration (CSC) on phenomenological energy fluxes per cross-section in *E. aureum* leaves: **(A)** ABS/CSm, **(B)** ET_o/CSm, **(C)** TR_o/CSm, and **(D)** DI_o/CSm. With rising CSC levels, absorbed, trapped, and transported energy fluxes (ABS/CSm, TR_o/CSm, ET_o/CSm) show a significant decline, while dissipated energy (DI_o/CSm) increases, indicating impaired photosynthetic efficiency under cigarette smoke-induced stress ($p < 0.05$).



suggests a progressive decline or decoupling of these fluorescence responses under prolonged high CSC exposure. In quadrant IV, most of the parameters form obtuse angles with the origin, indicating negative or weak correlation with CSC treatments at this later stage.

Overall, the PCA shows strong clustering and consistent correlation among biophysical parameters, as confirmed by the correlation matrix (refer to Figure 10).

The LD₅₀ and LD₉₀ values for *E. aureum*, which were calculated by number of mortality rate through probit analysis with a 95% probability level displays in Table 3. LD₅₀ and LD₉₀ represent the lethal dose necessary to cause 50% and 90% mortality, respectively. The values obtained for LD₅₀ is 6.4 CSC and LD₉₀ is 9.9 CSC.

4 Discussion

The detrimental effects of CS on the growth and physiological health of indoor plants are well-documented, with the extent of impact varying by plant species. In this study, exposure to low concentrations of CS (2 CSC) led to a minor reduction in the surface area of *E. aureum* plants. However, at higher concentrations (≥ 6 CSC), a significant decrease in surface area was observed. Previous study, by Prasad et al. (2015), have similarly reported that lower concentrations of cigarette butts (CBs) produce less pronounced effects, while higher concentrations (greater than 20 CBs) inhibit plant growth. Additionally, increased mortality rates were observed over time with higher CSC treatments, accompanied by a reduction in leaf number. This phenomenon is attributed to excessive exposure to CSC, which negatively affects plant survival. Moreover, gases from cigarette smoke, such as sulfur dioxide (SO₂),

nitrogen dioxide (NO₂), carbon radicals, ammonia, and volatile organic compounds, can be absorbed through the stomata of the leaves. These gases may damage the leaves and alter photosynthetic capacity, particularly at high concentrations (Permana et al., 2023).

Decreases in chlorophyll content can lead to a reduction in antenna size (Kirst et al., 2024; Martini et al., 2024). Strategic modulation of chlorophyll content or antenna size—such as reducing excess pigment to prevent light oversaturation under high light conditions—has been shown in some cases to enhance photosynthetic efficiency by minimizing energy loss and photo-inhibition. However, excessive reduction may impair light capture and thus negatively affect photosynthetic performance. At the canopy level, reduced leaf chlorophyll content can increase leaf transmittance, improve light distribution within the canopy, and thereby enhance canopy photosynthesis, as suggested by modeling studies (Song et al., 2021). Conversely, there are instances where chlorophyll-deficient mutants exhibit decreased photosynthetic rates. For example, the mutation of OsClp6 impairs the photosynthetic apparatus and chloroplast development (Dong et al., 2013). Similarly, the loss of the transcription factor OsPIL1 leads to a decrease in chlorophyll content, accompanied by a reduction in plant surface area (Mao et al., 2023). In our study, cigarette smoke exposure significantly reduced chlorophyll content in *E. aureum*, which was associated with a decline in photosynthetic efficiency and visible morphological stress, indicating the detrimental impact of smoke-induced chlorophyll loss on overall plant health.

The minimal fluorescence intensity values are a key indicator of the extent of irreversible damage to PSII, particularly to the light-harvesting complex II (LHCII). Such damage can hinder electron transfer on the reduced side of PSII (Goltsev et al., 2016; Kalaji et al.,

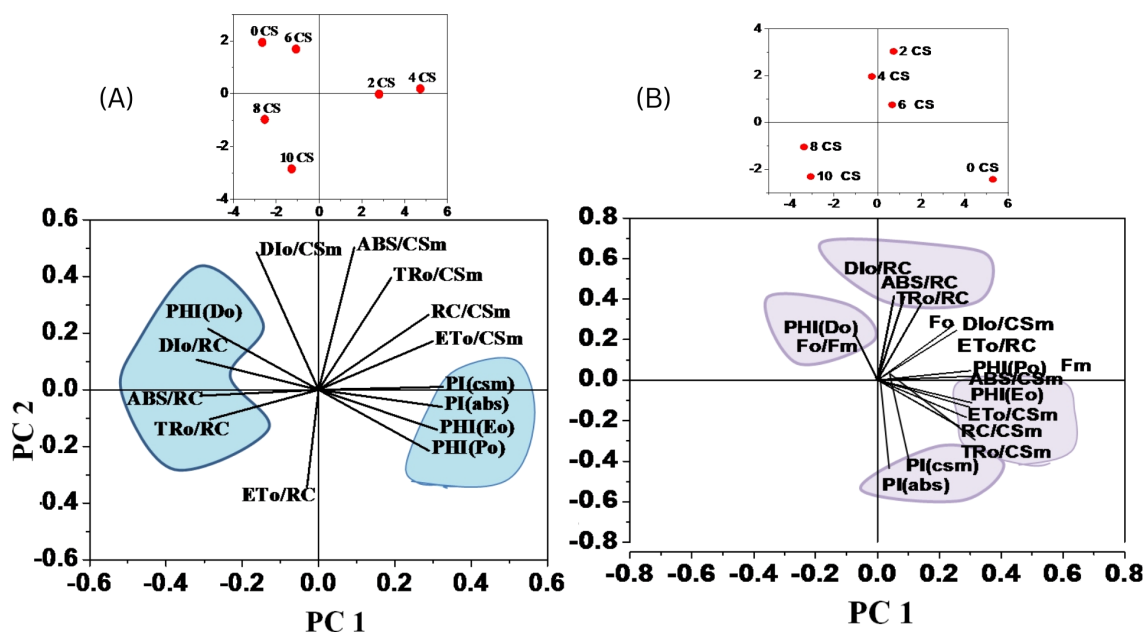


FIGURE 10 A heat map was used to illustrate the relative variability of multiple photosynthesis-related parameters obtained from the JIP test on *E. aureum* plants under CS stress. The data was collected for varying concentrations (0–10) after 24 hours, with orange indicating lower values (1%), yellow indicating medium (50%), and brown indicating the highest values (100%). Prior to color coding, all data was normalized to maintain unbiased results within a range of 1–100 for the parameter values. (A) relation after 3rd day (B) relation after end say of experiment (15th day).

TABLE 3 The probit analysis was used to determine the acute 48-hour LD₅₀ values of CS in *E. aureum* plants, along with their corresponding confidence limits.

		Confidence Limits		
Probit		95% Confidence Limits for concentration		
		Estimate	Lower Bound	Upper Bound
PROBIT	.010	.306	-9.713	2.897
	.020	1.031	-7.845	3.386
	.030	1.491	-6.666	3.702
	.040	1.837	-5.783	3.943
	.050	2.118	-5.068	4.143
	.060	2.358	-4.462	4.315
	.070	2.568	-3.932	4.468
	.080	2.756	-3.460	4.608
	.090	2.927	-3.033	4.736
	.100	3.085	-2.641	4.856
	.150	3.736	-1.042	5.376
	.200	4.255	.194	5.824
	.250	4.699	1.216	6.246
	.300	5.098	2.092	6.667
	.350	5.468	2.858	7.104
	.400	5.819	3.532	7.571
	.450	6.159	4.129	8.078
	.500	6.493	4.658	8.634
	.550	6.827	5.132	9.247
	.600	7.167	5.562	9.921
	.650	7.518	5.960	10.663
	.700	7.887	6.339	11.486
	.750	8.287	6.713	12.410
	.800	8.731	7.097	13.471
	.850	9.249	7.514	14.737
.900	9.901	8.007	16.363	
.910	10.058	8.123	16.759	
.920	10.230	8.247	17.191	
.930	10.418	8.381	17.668	
.940	10.628	8.530	18.201	
.950	10.867	8.698	18.812	
.960	11.149	8.893	19.532	
.970	11.495	9.130	20.420	
.980	11.955	9.441	21.604	
.990	12.680	9.924	23.477	

The logarithm used in the analysis was base 10.

2014). The disruption of the electron transport chain can be attributed to the degradation of the LHCII oligomer. Additionally, the presence of heavy metal ions in CS can enhance the dissipation of excitation energy as heat, a process known as non-photochemical quenching (Janeczko et al., 2005). A reduction in minimal fluorescence under high concentrations of cigarette smoke stress may indicate reduced PSII efficiency, likely due to conformational changes in the D1 protein induced by CS stress. These changes can alter the properties of PSII electron acceptors (Kalaji et al., 2014). Moreover, the presence of particulate matter in CS can limit the formation of PSI, PSII, and LHC complexes in *E. aureum*. Permana et al. (2023) conducted an experiment using CS exposure exclusively on *Calathea makoyana*. Their study demonstrated that prolonged exposure to CS under enclosed conditions resulted in visible chlorosis, reduced leaf turgor, and significant decreases in chlorophyll content, suggesting that CS-induced oxidative stress impairs photosynthetic efficiency and overall plant health. The oxygen-evolving complex within the PSII complex is essential for catalyzing redox reactions and splitting water during photosynthesis (Ifuku et al., 2010). This process produces dioxygen and hydrogen ions, which are necessary for ATP phosphorylation (Paul et al., 2022). Given the disruption of the photosynthetic apparatus by CS, our findings suggest that cigarette smoke stress may increase the physiological demand for water in *E. aureum*, as the plant attempts to compensate for impaired energy production by enhancing water-dependent processes such as ATP synthesis and organic compound biosynthesis. Water is a crucial component in plant physiological processes, especially photosynthesis (Treesubstorn et al., 2021).

The F_0/F_M ratio is an important parameter in the JIP test that indicates the efficiency of primary light energy conversion in the PSII reaction center (Baker et al., 2004; Kalaji et al., 2012; Schansker et al., 2005). It is commonly used as a stress indicator in various photosynthetic studies. This ratio depends on the fluorescence levels of F_0 and F_M , and any decrease in F_M can lead to a reduction in the F_0/F_M ratio with increasing levels of CSC. PCA reveals a positive correlation between dissipation per reaction center (DI_0/RC) and the F_0/F_M ratio. This indicates that as photochemical efficiency declines under CS stress, plants increasingly rely on non-photochemical energy dissipation pathways to protect the remaining functional PSII units. Such an increase in energy dissipation, reflected by higher DI_0/RC , has also been reported under various abiotic stresses, including heat, salinity, and drought, as a photoprotective mechanism (Kalaji et al., 2016). Therefore, the observed increase in both DI_0/RC and F_0/F_M under elevated CS concentrations suggests that CS imposes photoinhibitory pressure on PSII, and the plant attempts to mitigate this through increased energy dissipation. However, the observed increase in F_M values at early stages of 4–6 CSC treatments may appear contradictory. This anomaly could be due to transient photoprotective adjustments or measurement artifacts. The analysis of fluorescence transients, commonly known as the JIP test, in photosynthetic organisms exposed to abiotic stress, reveals a significant decrease in the ϕP_0 value. This reduction in ϕP_0 is due to a decline in the photochemical efficiency of PSII as a result of CS-induced stress. Under light conditions, the observed decrease in the maximum quantum yield

of PSII (ϕP_0) indicates that CS stress disrupts the redox reaction following Q_A and delays electron transport between Q_A^- and Q_B (Schansker et al., 2005). However, ϕP_0 alone provides only a partial understanding of PSII function. To more accurately assess the condition of the PSII acceptor side, additional parameters such as ϕE_0 (quantum yield of electron transport beyond Q_A^-) and ϕD_0 were also considered. In our study, ϕE_0 showed significant reductions at higher CS concentrations and prolonged exposure times, supporting the notion that CS stress impairs the electron transport between Q_A^- and Q_B . Conversely, ϕD_0 increased, suggesting enhanced energy dissipation mechanisms as a photoprotective response to CS stress. These combined changes indicate that CS negatively affects PSII function by disrupting the redox reactions at the acceptor side and enhancing energy dissipation to mitigate photodamage, as also supported by previous findings (Mykhaylenko and Zolotareva, 2017).

These fluorescence declines particularly in PI_{ABS} and ϕP_0 , are consistent with photoinhibition mechanisms that limit PSII efficiency under oxidative stress. Reactive oxygen species generated by CS exposure likely disrupt photosynthetic proteins and membranes, thereby reducing the plant's energy conversion capacity. Integrating these observations with oxidative stress markers would provide further clarity on the damage pathways. The ABS/RC ratio, which is determined by the total number of photons absorbed by chlorophyll molecules across all active reaction centers (RC) divided by the total number of active reaction centers, reflects the proportion of active versus inactive RCs. An increase in the number of active RCs leads to a higher ABS/RC ratio. Conversely, the TR_0/RC ratio measures the maximum rate at which excitons are captured by RC with a decrease in this ratio indicating a reduction in the population of the primary electron acceptor Q_A . An increased DI_0/RC ratio suggests a diminished amount of Q_A remaining in its reduced state. The analysis of specific energy flux reveals that various sites within PSII are sensitive to environmental stressors (Gautam et al., 2014; Zushi et al., 2012). The present study shows that with increasing concentrations of CS, the efficiency of electron trapping and transport in PSII declines, as active reaction RC are converted into inactive ones, thereby reducing the overall number of functional RCs. This decline in active RCs directly contributes to diminished photochemical efficiency and impaired electron transport. This decline is evident from the reductions in TR_0/CSm and ET_0/CSm values (Strasserf and Srivastava, 1995; Tsimilli-Michael, 2020; Zushi and Matsuzoe, 2017). A decrease in the ET_0/RC ratio indicates a reduced capacity for electron transport, as the inactive reaction centers are less capable of re-oxidizing the reduced Q_A (Rapacz et al., 2015). The DI_0/RC ratio, which represents the total dissipation of untrapped excitation energy per active RC, is influenced by the ratio of active to inactive RCs. Dissipation can occur through various pathways, including heat, fluorescence, and energy transfer to other systems. Despite variations in the active/inactive RC ratios, the DI_0/RC ratio remains relatively stable due to the effective utilization of energy by the active RCs (Grieco et al., 2015; Heber et al., 2011). Our results indicate that at higher CS concentrations (6, 8, and 10) during days 9, 12, and 15, the DI_0/RC ratio increases significantly. This suggests that under severe stress, the decline in active RCs surpasses the compensatory mechanisms, resulting in elevated energy dissipation per RC.

The phenomenological fluxes per cross-section—ABS/CSm, TR₀/CSm, ET₀/CSm, and DI₀/CSm—offer insights into the behavior of the entire PSII population rather than individual RCs. Under CS stress, ABS/CSm and TR₀/CSm declined, implying impaired light absorption and trapping capacity across the PSII antenna system. The reduction in ET₀/CSm further supports the view that CS impairs the linear electron transport chain, compromising the energy transduction processes essential for ATP and NADPH production (Kalaji et al., 2014; Stirbet et al., 2018). In contrast, DI₀/CSm increased with CS exposure, indicating a shift toward energy dissipation as heat or fluorescence, a typical response to protect the remaining functional PSII units from excess excitation pressure (Yusuf et al., 2010).

The performance index of a plant is a sensitive indicator of stress effects on its physiological components. This index is calculated using parameters based on energy absorption (PI_{ABS}) and cross-section (PI_{CS}), with PI_{CS} being dependent on phenomenological energy flux (Baker et al., 2004; Srivastava and Strasser, 1999). The performance index integrates multiple factors including the density of reaction centers, trapping efficiency, and electron transport efficiency, analogous to the Goldman equation (Goldman, 1943). In our study, exposure to CS significantly reduced the PI_{ABS} and PI_{CS} values in *E. aureum*. The decline in PI_{ABS} is linked to decreased activity of the RC, which in turn diminishes the overall efficiency of these centers (Kalaji et al., 2014, 2017; Kumar et al., 2020). The efficiency of electron trapping during the light reactions is crucial for plant productivity, as it directly impacts the plant's ability to generate energy for growth and development (Sharma et al., 2023; Zhang et al., 2018). Through statistical analyses, including PCA and correlation matrices, we identified several JIP test parameters—such as ABS/CSm, TR₀/CSm, ET₀/CSm, φP₀, PI_{ABS}, and PI_{CS}—that exhibited a dose-dependent response to CS stress. Additionally, probit analysis of the LD₅₀ values revealed that CS is highly toxic to *E. aureum*. LD₅₀ of approximately 6.49, indicating that moderate levels of cigarette smoke can cause lethal stress in 50% of *E. aureum* plants. Early effects begin at lower concentrations (LD₁₀ ≈ 3.08), suggesting high sensitivity to smoke exposure. The steep rise in mortality beyond LD₅₀ highlights a dose-dependent toxicity pattern. These findings emphasize the harmful impact of cigarette smoke on indoor plants even at sub-lethal levels.

5 Conclusion

In conclusion, this study reveals the detrimental effects of CS on *Epipremnum aureum*, a commonly used indoor plant, highlighting the broader implications for indoor air quality and plant health. Our findings indicate that exposure to CS induces significant morphological alterations, leaf damage, and reduced overall vigor. These physical changes are accompanied by a reduction in chlorophyll content, measured using the Arnon (1949) method, and a decrease in photosynthetic efficiency, as indicated by changes in chlorophyll fluorescence parameters analyzed using Biolyzer software. These are important indicators of the plant's overall health and vitality. The research shows a clear dose-response

relationship, with higher concentrations of CS causing more severe damage, ultimately leading to plant mortality. This underscores the severe impact of CS, not only on plant life but also on the effectiveness of indoor plants in air purification. The results emphasize the necessity for improved indoor air quality management, particularly in environments where cigarette smoking is prevalent. By documenting these adverse effects, this study highlights the importance of using indoor plants as bio-indicators for air pollution and advocates for policies and practices aimed at reducing indoor pollutant levels. The evidence presented highlights the urgent need for a more integrated approach to managing indoor air quality, emphasizing its impact on both plant health and human well-being. Although research on plant–smoke interactions remains limited, our study contributes valuable insights to this emerging field. The observed effects of CS on indoor vegetation underline the importance of implementing stricter air quality regulations in enclosed environments where smoking occurs. To build on these findings, future research should incorporate molecular, physiological, and biochemical approaches to deepen our understanding of how airborne pollutants affect plant systems.

Data availability statement

The original contributions presented in the study are included in the article/Supplementary Material. Further inquiries can be directed to the corresponding author.

Author contributions

GS: Investigation, Writing – original draft, Formal analysis. UB: Methodology, Investigation, Writing – review & editing. HS: Writing – original draft, Data curation, Formal analysis. HDC: Writing – review & editing, Software. VS: Conceptualization, Methodology, Supervision, Writing – review & editing.

Funding

The author(s) declare that no financial support was received for the research and/or publication of this article.

Acknowledgments

Author would like to acknowledge Mohanlal Sukhadia University, Udaipur for providing lab facilities.

Conflict of interest

The authors declare that the research was conducted in the absence of any commercial or financial relationships that could be construed as a potential conflict of interest.

Generative AI statement

The author(s) declare that no Generative AI was used in the creation of this manuscript.

Publisher's note

All claims expressed in this article are solely those of the authors and do not necessarily represent those of their affiliated organizations,

or those of the publisher, the editors and the reviewers. Any product that may be evaluated in this article, or claim that may be made by its manufacturer, is not guaranteed or endorsed by the publisher.

Supplementary material

The Supplementary Material for this article can be found online at: <https://www.frontiersin.org/articles/10.3389/fpls.2025.1595713/full#supplementary-material>

References

- Aksoy, S. A., Kiziltan, A., Kiziltan, M., Köksal, M. A., Öztürk, F., Tekeli, Ş. E., et al. (2021). Mortality and morbidity costs of road traffic-based air pollution in Turkey. *J. Transport. Health* 22, 101142. doi: 10.1016/j.jth.2021.101142
- Arnon, D. I. (1949). Copper enzymes in isolated chloroplasts: polyphenoloxidase in *Beta vulgaris*. *Plant Physiology* 24 (1), 1–15. doi: 10.1104/pp.24.1.1
- Ashraf, S., Ali, Q., Zahir, Z. A., Ashraf, S., and Asghar, H. N. (2019). Phytoremediation: Environmentally sustainable way for reclamation of heavy metal polluted soils. *Ecotoxicol. Environ. Saf.* 174, 714–727. doi: 10.1016/j.ecoenv.2019.02.068
- Baker, R. R., da Silva, J. R. P., and Smith, G. (2004). The effect of tobacco ingredients on smoke chemistry. Part I: Flavourings and additives. *Food Chem. Toxicol.* 42, 3–37. doi: 10.1016/S0278-6915(03)00189-3
- Basu, S., Sengupta, R., and Zandi, P. (2014). "Arecaceae: The majestic family of palms," in *The Encyclopedia of Earth* (Washington, DC, USA: Environmental Information Coalition, National Council for Science and Environment).
- Bennet, R. J., Breen, C. M., and Fey, M. V. (1987). The effects of aluminium on root cap function and root development in *Zea mays* L. *Environ. Exp. Bot.* 27, 91–104. doi: 10.1016/0098-8472(87)90059-1
- Benson, N. F., Floyd, R. G., Kranzler, J. H., Eckert, T. L., Fefer, S. A., and Morgan, G. B. (2019). Test use and assessment practices of school psychologists in the United States: Findings from the 2017 National Survey. *J. School. Psychol.* 72, 29–48. doi: 10.1016/j.jsp.2018.12.004
- Berglund, B., Brunekreef, B., Knöppe, H., Lindvall, T., Maroni, M., Mølhav, L., et al. (1992). Effects of indoor air pollution on human health. *Indoor. Air.* 2, 2–25. doi: 10.1111/j.1600-0668.1992.02-21.x
- Blount, R. J., Phan, H., Trinh, T., Dang, H., Merrifield, C., Zavala, M., et al. (2021). Indoor air pollution and susceptibility to tuberculosis infection in urban Vietnamese children. *Am. J. Respir. Crit. Care Med.* 204, 1211–1221. doi: 10.1164/rccm.202101-0136OC
- Brilli, F., Fares, S., Ghirardo, A., de Visser, P., Calatayud, V., Muñoz, A., et al. (2018). Plants for sustainable improvement of indoor air quality. *Trends Plant Sci.* 23, 507–512. doi: 10.1016/j.tplants.2018.03.004
- Caselli, M., de Gennaro, G., Marzocca, A., Trizio, L., and Tutino, M. (2010). Assessment of the impact of the vehicular traffic on BTEX concentration in ring roads in urban areas of Bari (Italy). *Chemosphere* 81, 306–311. doi: 10.1016/j.chemosphere.2010.07.033
- Cetin, M., Onac, A. K., Sevik, H., and Sen, B. (2019). Temporal and regional change of some air pollution parameters in Bursa. *Air. Quality. Atmosphere. Health* 12, 311–316. doi: 10.1007/s11869-018-00657-6
- Dávila-Román, V. G., Toenjes, A. K., Meyers, R. M., Lenzen, P. M., Simkovich, S. M., Herrera, P., et al. (2021). Ultrasound Core Laboratory for the Household Air Pollution Intervention Network Trial: standardized training and image management for field studies using portable ultrasound in fetal, lung, and vascular evaluations. *Ultrasound. Med. Biol.* 47, 1506–1513. doi: 10.1016/j.ultrasmedbio.2021.02.015
- de Vries, W. (2021). Impacts of nitrogen emissions on ecosystems and human health: A mini review. *Curr. Opin. Environ. Sci. Health* 21, 100249. doi: 10.1016/j.coesh.2021.100249
- Dobaradaran, S., Soleimani, F., Akhbarzadeh, R., Schmidt, T. C., Marzban, M., and Basirian Jahromi, R. (2021). Environmental fate of cigarette butts and their toxicity in aquatic organisms: A comprehensive systematic review. *Environ. Res.* 195, 110881. doi: 10.1016/j.envres.2021.110881
- Dong, H., Fei, G.-L., Wu, C.-Y., Wu, F.-Q., Sun, Y.-Y., Chen, M.-J., et al. (2013). A rice virescent-yellow leaf mutant reveals new insights into the role and assembly of plastid caseinolytic protease in higher plants. *Plant Physiol.* 162, 1867–1880. doi: 10.1104/pp.113.217604
- Fix, B. (2019). Energy, hierarchy and the origin of inequality. *PLoS One* 14, e0215692. doi: 10.1371/journal.pone.0215692
- Forster, M., Fiebelkorn, S., Yurteri, C., Mariner, D., Liu, C., Wright, C., et al. (2018). Assessment of novel tobacco heating product THP1. 0. Part 3: Comprehensive chemical characterisation of harmful and potentially harmful aerosol emissions. *Regul. Toxicol. Pharmacol.* 93, 14–33. doi: 10.1016/j.yrtph.2017.10.006
- Gautam, A., Agrawal, D., SaiPrasad, S. V., and Jajoo, A. (2014). A quick method to screen high and low yielding wheat cultivars exposed to high temperature. *Physiol. Mol. Biol. Plants* 20, 533–537. doi: 10.1007/s12298-014-0252-4
- Goldman, D. E. (1943). Potential, impedance, and rectification in membranes. *J. Gen. Physiol.* 27, 37–60. doi: 10.1085/jgp.27.1.37
- Goltsev, V. N., Kalaji, H. M., Paunov, M., Bąba, W., Horaczek, T., Mojski, J., et al. (2016). Variable chlorophyll fluorescence and its use for assessing physiological condition of plant photosynthetic apparatus. *Russian J. Plant Physiol.* 63, 869–893. doi: 10.1134/S1021443716050058
- Gomez-Flores, A., Bradford, S. A., Cai, L., Urik, M., and Kim, H. (2023). Prediction of attachment efficiency using machine learning on a comprehensive database and its validation. *Water Res.* 229, 119429. doi: 10.1016/j.watres.2022.119429
- Gorena, T., Fadic, X., and Cereceda-Balic, F. (2020). Cupressus macrocarpa leaves for biomonitoring the environmental impact of an industrial complex: The case of Puchuncavi-Ventanas in Chile. *Chemosphere* 260, 127521. doi: 10.1016/j.chemosphere.2020.127521
- Grieco, M., Suorsa, M., Jajoo, A., Tikkanen, M., and Aro, E.-M. (2015). Light-harvesting II antenna trimers connect energetically the entire photosynthetic machinery—including both photosystems II and I. *Biochim. Biophys. Acta (BBA)-Bioenerget.* 1847, 607–619. doi: 10.1016/j.bbabi.2015.03.004
- Gushit, J. S., Mohammed, S. U., and Moda, H. M. (2022). Indoor air quality monitoring and characterization of airborne workstations pollutants within detergent production plant. *Toxics* 10, 419. doi: 10.3390/toxics10080419
- Hatami-Manesh, M., Mortazavi, S., Solgi, E., and Mohtadi, A. (2021). Assessing the uptake and accumulation of heavy metals and particulate matter from ambient air by some tree species in Isfahan Metropolis, Iran. *Environ. Sci. Pollut. Res.* 28, 41451–41463. doi: 10.1007/s11356-021-13524-2
- Heber, U., Soni, V., and Strasser, R. J. (2011). Photoprotection of reaction centers: thermal dissipation of absorbed light energy vs charge separation in lichens. *Physiol. Plant.* 142, 65–78. doi: 10.1111/j.1399-3054.2010.01417.x
- Ifuku, K., Ishihara, S., and Sato, F. (2010). Molecular functions of oxygen-evolving complex family proteins in photosynthetic electron flow. *J. Integr. Plant Biol.* 52, 723–734. doi: 10.1111/j.1744-7909.2010.00976.x
- Isinkaralar, K., Isinkaralar, O., and Bayraktar, E. P. (2024). Ecological and health risk assessment in road dust samples from various land use of Düzce City Center: Towards the sustainable urban development. *Water. Air. Soil Pollut.* 235, 84. doi: 10.1007/s11270-023-06879-4
- Janeczko, A., Koscielniak, J., Pilipowicz, M., Szarek-Lukaszewska, G., and Skoczowski, A. (2005). Protection of winter rape photosystem 2 by 24-epi brassinolide under cadmium stress. *Photosynthetica* 43, 293–298. doi: 10.1007/s11099-005-0048-4
- Kalaji, H. M., Goltsev, V., Bosa, K., Allakhverdiev, S. I., and Strasser, R. J. (2012). Experimental *in vivo* measurements of light emission in plants: a perspective dedicated to David Walker. *Photosynthesis. Res.* 114, 69–96. doi: 10.1007/s11220-012-9780-3
- Kalaji, H. M., Jajoo, A., Oukarroum, A., Brestic, M., Zivcak, M., Samborska, I. A., et al. (2016). Chlorophyll a fluorescence as a tool to monitor physiological status of plants under abiotic stress conditions. *Acta Physiol. Plant.* 38, 1–11. doi: 10.1007/s11738-016-2113-y
- Kalaji, H. M., Schansker, G., Brestic, M., Bussoiti, F., Calatayud, A., Ferroni, L., et al. (2017). Frequently asked questions about chlorophyll fluorescence, the sequel. *Photosynthesis. Res.* 132, 13–66. doi: 10.1007/s11220-016-0318-y
- Kalaji, H. M., Schansker, G., Ladle, R. J., Goltsev, V., Bosa, K., Allakhverdiev, S. I., et al. (2014). Frequently asked questions about *in vivo* chlorophyll fluorescence: practical issues. *Photosynthesis. Res.* 122, 121–158. doi: 10.1007/s11220-014-0024-6

- Kirst, M., Perron, N., Dervinis, C., Pereira, W., and Barbazuk, W. (2024). *Mesophyll-Specific Circadian Dynamics of CAM Induction in the Ice Plant Unveiled by Single-Cell Transcriptomics* (Durham, NC, USA: Research Square). doi: 10.21203/rs.3.rs-3783761/v1
- Kumakli, H., A'ja, V. D., McDaniel, K., Mehari, T. F., Stephenson, J., Maple, L., et al. (2017). Environmental biomonitoring of essential and toxic elements in human scalp hair using accelerated microwave-assisted sample digestion and inductively coupled plasma optical emission spectroscopy. *Chemosphere* 174, 708–715. doi: 10.1016/j.chemosphere.2017.02.032
- Kumar, D., Singh, H., Raj, S., and Soni, V. (2020). Chlorophyll a fluorescence kinetics of mung bean (*Vigna radiata* L.) grown under artificial continuous light. *Biochem. Biophys. Rep.* 24, 100813. doi: 10.1016/j.bbrep.2020.100813
- Liao, L., Du, M., and Chen, Z. (2021). Air pollution, health care use and medical costs: Evidence from China. *Energy Econ.* 95, 105132. doi: 10.1016/j.eneco.2021.105132
- Mao, L., Song, Q., Li, M., Liu, X., Shi, Z., Chen, F., et al. (2023). Decreasing photosystem antenna size by inhibiting chlorophyll synthesis: A double-edged sword for photosynthetic efficiency. *Crop Environ.* 2, 46–58. doi: 10.1016/j.crope.2023.02.006
- Martini, D., Sakowska, K., Migliavacca, M., Julitta, T., Hammerle, A., Schwarz, M., et al. (2024). *Introducing AustroSIF: A compilation of combined passive and active fluorescence data at flux tower sites across Europe; dataset overview and potential applications (presentation at Copernicus Meetings - EGU General Assembly 2024, Austria Center Vienna, Vienna, Austria) 14 -19 April 2024*. (Göttingen, Germany: Copernicus Meetings). doi: 10.5194/egusphere-egu24-18884
- Mason, R. P., Lawson, N. M., and Sheu, G. R. (2000). Annual and seasonal trends in mercury deposition in Maryland. *Atmospheric Environ.* 34, 1691–1701. doi: 10.1016/S1352-2310(99)00428-8
- Miranda, A. F., Kumar, N. R., Spangenberg, G., Subudhi, S., Lal, B., and Mouradov, A. (2020). Aquatic plants, *Landoltia punctata*, and *Azolla filiculoides* as bio-converters of wastewater to biofuel. *Plants* 9, 437. doi: 10.3390/plants9040437
- Mykhaylenko, N. F., and Zolotareva, E. K. (2017). The effect of copper and selenium nanocarboxylates on biomass accumulation and photosynthetic energy transduction efficiency of the green algae *Chlorella vulgaris*. *Nanoscale Res. Lett.* 12, 147. doi: 10.1186/s11671-017-1914-2
- Obore, N., Kawuki, J., Guan, J., Papabathini, S. S., and Wang, L. (2020). Association between indoor air pollution, tobacco smoke and tuberculosis: an updated systematic review and meta-analysis. *Public Health* 187, 24–35. doi: 10.1016/j.puhe.2020.07.031
- Organization, W. H. (2018). *Air pollution and child health: prescribing clean air: summary* (World Health Organization).
- Organization, W. H. and others (2015). *WHO global report on trends in prevalence of tobacco smoking 2015* (World Health Organization).
- Paul, R., Banerjee, S., Sen, S., Dubey, P., Maji, S., Bachhawat, A. K., et al. (2022). A novel leishmanial copper P-type ATPase plays a vital role in parasite infection and intracellular survival. *J. Biol. Chem.* 298. doi: 10.1016/j.jbc.2021.101539
- Percival, G. C., Keary, I. P., and Sulaiman, A.-H. (2006). An assessment of the drought tolerance of *Fraxinus* genotypes for urban landscape plantings. *Urban. Forestry. Urban. Greening*, 5, 17–27. doi: 10.1016/j.ufug.2006.03.002
- Permana, B. H., Nookongbut, P., Krobthong, S., Yingchutrakul, Y., Saithong, T., Thiravetyan, P., et al. (2023). Comparative proteomics analysis of the responses to cigarette smoke particulate matter in six plant species leaves (Durham, NC, USA: Research Square). doi: 10.21203/rs.3.rs-3783761/v1
- Prasad, S. M., Singh, A., and Singh, P. (2015). Physiological, biochemical and growth responses of *Azolla pinnata* to chlorpyrifos and cypermethrin pesticides exposure: a comparative study. *Chem. Ecol.* 31, 285–298. doi: 10.1080/02757540.2014.950566
- Pryor, W. A., and Stone, K. (1993). Oxidants in cigarette smoke radicals, hydrogen peroxide, peroxyxynitrate, and peroxyxynitrite. *A. Ann. New York Acad. Sci.* 686, 12–27. doi: 10.1111/j.1749-6632.1993.tb39148.x
- Rajagopalan, P., and Goodman, N. (2021). Improving indoor air quality of residential buildings during bushfire smoke events. *Climate* 2021 9, 32. doi: 10.3390/cli9020032 s Note: MDPI stays neutral with regard to jurisdictional claims in ...
- Rapacz, M., Sasal, M., Kalaji, H. M., and Kościelniak, J. (2015). Is the OJIP test a reliable indicator of winter hardiness and freezing tolerance of common wheat and triticale under variable winter environments? *PLoS One* 10, e0134820. doi: 10.1371/journal.pone.0134820
- Rumchev, K., Zhao, Y., and Spickett, J. (2017). Health risk assessment of indoor air quality, socioeconomic and house characteristics on respiratory health among women and children of Tirupur, South India. *Int. J. Environ. Res. Public Health* 14, 429. doi: 10.3390/ijerph14040429
- Rupakheti, D., Yin, X., Rupakheti, M., Zhang, Q., Li, P., Rai, M., et al. (2021). Spatio-temporal characteristics of air pollutants over Xinjiang, northwestern China. *Environ. Pollut.* 268, 115907. doi: 10.1016/j.envpol.2020.115907
- Sangani, M. F., Owens, G., Nazari, B., Astaraei, A., Fotovat, A., and Emami, H. (2019). Different modelling approaches for predicting titanium dioxide nanoparticles mobility in intact soil media. *Sci. Total Environ.* 665, 1168–1181. doi: 10.1016/j.scitotenv.2019.01.345
- Schansker, G., Tóth, S. Z., and Strasser, R. J. (2005). Methylviologen and dibromothymoquinone treatments of pea leaves reveal the role of photosystem I in the Chl a fluorescence rise OJIP. *Biochim. Biophys. Acta (BBA)-Bioenerget.* 1706, 250–261. doi: 10.1016/j.bbabi.2004.11.006
- Shahid, I., Kistler, M., Shahid, M. Z., and Puxbaum, H. (2019). Aerosol chemical characterization and contribution of biomass burning to particulate matter at a residential site in Islamabad, Pakistan. *Aerosol. Air. Qual. Res.* 19, 148–162. doi: 10.4209/aaqr.2017.12.0573
- Sharma, J., Shah, G., Strasser, R. J., and Soni, V. (2023). Effects of malachite green on biochemistry and photosystem II photochemistry of *Eichhornia crassipes*. *Funct. Plant Biol.* 50, 663–675. doi: 10.1071/FP23094
- Song, D., Gao, D., Sun, H., Qiao, L., Zhao, R., Tang, W., et al. (2021). Chlorophyll content estimation based on cascade spectral optimizations of interval and wavelength characteristics. *Comput. Electron. Agric.* 189, 106413. doi: 10.1016/j.compag.2021.106413
- Srivastava, A., and Strasser, R. J. (1999). Greening of peas: parallel measurements of 77 K emission spectra, OJIP chlorophyll a fluorescence transient, period four oscillation of the initial fluorescence level, delayed light emission, and P700. *Photosynthetica* 37, 365–392. doi: 10.1023/A:1007199408689
- Stirbet, A., Lázár, D., Kromdijk, J., and Govindjee, (2018). Chlorophyll a fluorescence induction: can just a one-second measurement be used to quantify abiotic stress responses? *Photosynthetica* 56, 86–104. doi: 10.1007/s11099-018-0770-3
- Strasser, R. (1992). "On the OJIP fluorescence transient in leaves and D1 mutants of *Chlamydomonas reinhardtii*," in *Research in Photosynthesis: Proceedings of the IXth International Congress on Photosynthesis*, ed. N. Murada. (Dordrecht, The Netherlands: Kluwer Academic Publishers), vol. 2, 29–32.
- Strasser, R. J., Srivastava, A., and Tsimilli-Michael, M. (2000). "The fluorescence transient as a tool to characterize and screen photosynthetic samples," in *Probing Photosynthesis: Mechanisms, Regulation and Adaptation*, eds. m. Yunus, E. Pathre and P. Mohanty. (London, UK: Taylor & Francis), 445–483.
- Strasser, R. J., and Srivastava, A. (1995). Polyphasic chlorophyll a fluorescence transient in plants and cyanobacteria. *Photochem. Photobiol.* 61, 32–42. doi: 10.1111/j.1751-1097.1995.tb02940.x
- Tarin-Carrasco, P., Im, U., Geels, C., Palacios-Peña, L., and Jiménez-Guerrero, P. (2021). Contribution of fine particulate matter to present and future premature mortality over Europe: A non-linear response. *Environ. Int.* 153, 106517. doi: 10.1016/j.envint.2021.106517
- Treesubuntorn, C., Setiawan, G. D., Permana, B. H., Citra, Y., Krobthong, S., Yingchutrakul, Y., et al. (2021). Particulate matter and volatile organic compound phytoremediation by perennial plants: Affecting factors and plant stress response. *Sci. Total Environ.* 794, 148779. doi: 10.1016/j.scitotenv.2021.148779
- Tsimilli-Michael, M. (2020). Revisiting JIP-test: An educative review on concepts, assumptions, approximations, definitions and terminology. *Photosynthetica* 58, 275–292. doi: 10.32615/ps.2019.150
- Viana, F. (2011). Chemosensory properties of the trigeminal system. *ACS Chem. Neurosci.* 2, 38–50. doi: 10.1021/cn100102c
- Vimercati, L., Baldassarre, A., Gatti, M. F., Gagliardi, T., Serinelli, M., De Maria, L., et al. (2016). Non-occupational exposure to heavy metals of the residents of an industrial area and biomonitoring. *Environ. Monit. Assess.* 188, 1–13. doi: 10.1007/s10661-016-5693-5
- Wood, R. A., Burchett, M. D., Alquezar, R., Orwell, R. L., Tarran, J., and Torpy, F. (2006). The potted-plant microcosm substantially reduces indoor air VOC pollution: I. Office field-study. *Water. Air. Soil Pollut.* 175, 163–180. doi: 10.1007/s11270-006-9124-z
- Yadav, S. K. (2010). Heavy metals toxicity in plants: an overview on the role of glutathione and phytochelatin in heavy metal stress tolerance of plants. *South Afr. J. Bot.* 76, 167–179. doi: 10.1016/j.sajb.2009.10.007
- Yusuf, M. A., Kumar, D., Rajwanshi, R., Strasser, R. J., Tsimilli-Michael, M., and Sarin, N. B. (2010). Overexpression of γ -tocopherol methyl transferase gene in transgenic *Brassica juncea* plants alleviates abiotic stress: physiological and chlorophyll a fluorescence measurements. *Biochim. Biophys. Acta (BBA)-Bioenerget.* 1797, 1428–1438. doi: 10.1016/j.bbabi.2010.02.002
- Zacarias, L. M., and Grubert, E. (2021). Effects of implausible power plant lifetime assumptions on US federal energy system projected costs, greenhouse gas emissions, air pollution, and water use. *Environ. Res.: Infrastruct. Sustainabil.* 1, 11001. doi: 10.1016/j.rser.2022.112208
- Zai, X. M., Zhu, S. N., Qin, P., Wang, X. Y., Che, L., and Luo, F. X. (2012). Effect of *Glomus mosseae* on chlorophyll content, chlorophyll fluorescence parameters, and chloroplast ultrastructure of beach plum (*Prunus maritima*) under NaCl stress. *Photosynthetica* 50, 323–328. doi: 10.1007/s11099-012-0035-5
- Zhang, J., Zhang, H., Srivastava, A. K., Pan, Y., Bai, J., Fang, J., et al. (2018). Knockdown of rice microRNA166 confers drought resistance by causing leaf rolling and altering stem xylem development. *Plant Physiol.* 176, 2082–2094. doi: 10.1104/pp.17.01432
- Zushi, K., Kajiwar, S., and Matsuzoe, N. (2012). Chlorophyll a fluorescence OJIP transient as a tool to characterize and evaluate response to heat and chilling stress in tomato leaf and fruit. *Sci. Hortic.* 148, 39–46. doi: 10.1016/j.scienta.2012.09.022
- Zushi, K., and Matsuzoe, N. (2017). Using of chlorophyll a fluorescence OJIP transients for sensing salt stress in the leaves and fruits of tomato. *Sci. Hortic.* 219, 216–221. doi: 10.1016/j.scienta.2017.03.016